ENCLOSURE 5

MFN 15-056

NEDO-33376, Revision 2,
"LANCR02 Lattice Physics Model Description"

Non-Proprietary Information - Class I (Public)

IMPORTANT NOTICE

This is a non-proprietary version of Enclosure 4, from which has the proprietary information has been removed. Portions of the enclosure that have been removed are indicated by an open and closed bracket as shown here [[ ]].

Global Nuclear Fuel

A Joint Venture of GE, Toshiba, & Hitachi

NEDO-33376
Revision 2
August 2015

Non-Proprietary Information – Class I (Public)

Licensing Topical Report

LANCR02 LATTICE PHYSICS MODEL DESCRIPTION

INFORMATION NOTICE

This is a non-proprietary version of the document NEDC-33376P, Revision 2, which has the proprietary information removed. Portions of the document that have been removed are indicated by an open and closed bracket as shown here [[ ]].

IMPORTANT NOTICE REGARDING THE CONTENTS OF THIS REPORT PLEASE READ CAREFULLY

The only undertakings of (GNF) with respect to information in this document are contained in contracts between GNF and its customers, and nothing contained in this document shall be construed as changing those contracts. The use of this information by anyone other than those participating entities and for any purposes other than those for which it is intended is not authorized; and with respect to any unauthorized use, GNF makes no representation or warranty, and assumes no liability as to the completeness, accuracy, or usefulness of the information contained in this document.

Revision Status

Revision	Description of Change
0	GNF Internal Document
1	Initial Submittal to NRC
2	Updates following NRC request for additional information

Table of Contents

List of Figures

List of Tables

1. INTRODUCTION

1.1. Purpose and scope

LANCR02 is an Engineering Computer Program (ECP) that enables the detailed nuclear design and evaluation of BWR fuel lattices using a characteristics transport method as the basis for solution. LANCR02 incorporates features that support design, evaluation, and verification of the nuclear characteristics of BWR fuel lattices.

1.2. Features

The function of LANCR02 is to compute the lattice nuclear characteristics and to generate the fuel assembly nuclear parameters for use in downstream applications, such as 3-D nodal simulators and transient analysis codes.

1.3. The LANCR02 Code System

LANCR02 is written as a collection of individual modules. Each module performs a specific function and information is passed from one module to the next. LANCR02 modules and their functions are as follows:

User Input Module
: This module reads a set of inputs consisting of geometry inputs, rod locations, enrichment location assignments, lattice state conditions, geometry descriptions, as well as all available switches.

Geometry Setting Module
: This module prepares the geometrical data required for subsequent calculations in LANCR02. Variables for defining cell boundaries, geometrical configuration within cells, and material compositions are provided.

Cross Section Processing Module
: This module reads the fine-group neutron cross section library for all requested isotopes.

Spectrum Calculation Module
: This module calculates weighting functions (i.e., flux spectra) that will be used to condense the fine-group macroscopic cross sections to a coarser energy group structure for the two-dimensional transport calculation.

Neutron Transport Module
: This module solves the two-dimensional Boltzmann transport equation using the Method of Characteristics to obtain a detailed flux distribution in each region of the lattice.

Gamma Transport Module

This module calculates a gamma source distribution using the neutron flux distribution obtained from the coarse group neutron transport module. The fixed-source Boltzmann transport equation is solved using the Method of Characteristics to obtain a detailed gamma flux in each region of the lattice. The gamma distribution is used to determine the gamma energy deposition in each region of the lattice and a gamma detector response in the corner of the lattice.

Output Module

This module provides all the output quantities needed by the core simulator, as well as ASCII output for printing.

Depletion Module

This module performs isotopic depletion calculations for either the fuel materials in fuel rods or the poison materials (B-10 and Hf) in control blades, or both.

2. METHODOLOGY

This section of the report presents a description of the theory and models that form the computational basis for the LANCR02 methodology. Qualification of the methodology is part of the LANCR02 Lattice Physics Qualification LTR (NEDC-33377P).

Many of the LANCR02 physics models are described in the open literature in [1]. However, this report should be considered as the official LANCR02 methodology description.

2.1. Fine-group cross sections

The LANCR02 calculation begins by retrieving microscopic cross section data from a fine-group, energy-dependent cross section library. The library includes more than 100 energy groups and more than 200 individual isotopes and mixtures. A list of the isotopes and the details of the LANCR02 libraries is included in Appendix A.

This sub-section describes the method used for obtaining microscopic cross sections from the library for each isotope in each material region of the lattice.

The multi-group cross section library for LANCR02 can be created by a standard method such as NJOY [2]. To produce a multi-group library from the continuous-energy data, a flux spectrum is needed to combine pointwise data over an energy range,

$$\sigma_x^g = \frac{\int_E^{E+\Delta E} \sigma_x(E)\phi(E)dE}{\int_E^{E+\Delta E} \phi(E)dE} \tag{1}$$

where x is a reaction type (e.g., fission, capture, etc.); g is a fine energy group covering the energy interval E to $E+\Delta E$; $\sigma_x(E)$ is the microscopic cross section at energy point E; and $\phi(E)$ is the flux spectrum used to weight the continuous-energy cross section over the energy interval from E to $E+\Delta E$.

The flux in Eq. (1) is meant to represent the spectrum found in a typical BWR. To obtain this, it is assumed that the magnitude of the flux is inversely proportional to the energy of the neutrons,

$$\phi(E) \propto \frac{1/E}{\sigma_{t,iso}(E)+\sigma_0} \tag{2}$$

where $\sigma_{t,iso}(E)$ is the microscopic total cross section for the isotope under consideration, *iso*; and σ_0 is a microscopic background cross section. Eq. (2) is often referred to as the Bondarenko model and is based on the Narrow Resonance (NR) approximation. The total cross section in the denominator of Eq. (2) is used to create flux dips surrounding resonances,

while the background cross section is used to account for scattering by all other isotopes in the fuel mixture and may be thought of as a dilution factor of $\sigma_{t,iso}(E)$. That is, the larger the value of σ_0 becomes, the more "dilute" the value of $\sigma_{t,iso}(E)$ becomes in the sum of $\sigma_{t,iso}(E)+\sigma_0$. When $\sigma_0 >> \sigma_{t,iso}(E)$, the value of $\sigma_{t,iso}(E)$ is insignificant and this condition is referred to as being "infinitely dilute."

For each isotope in the LANCR02 cross section library, the NR approximation is used to create a base cross section set at 293K for infinitely dilute conditions by setting σ_0 equal to a very large value in Eq. (2) (i.e., $\sigma_0 >> \sigma_{t,iso}(E)$, representing a resonance absorber present in such small abundance that the resonances do not affect the flux spectrum).

For each isotope iso, reaction x, group g, temperature T, and background cross section σ_0 an f-table is constructed with NJOY data using the definition:

$$f^g_{x,iso}(T,\sigma_0) = \frac{\sigma^g_{x,iso}(T,\sigma_0)}{\sigma^g_{x,iso}(293K,\infty)}$$

This operation is performed (library preprocessing) for a number of temperatures (e.g., 293K, 373K, 559K, 748K, 793K, 833K, 963K, 1273K, 1773K and 2573K) and background cross sections (e.g. 1E+10, 1E+6, 1E+5, 1E+4, 1E+3, and 1E+2 barns), depending on the type of isotope, forming a discrete two-dimensional table for every cross section type per isotope. For a given cross section at a specific temperature and background cross section, the corresponding two-dimensional f-table is then interpolated to extract the correct cross section according to:

$$\sigma^g_{x,iso}(T,\sigma_0) = \sigma^g_{x,iso}(293K,\infty)\cdot f^g_{x,iso}(T,\sigma_0) \quad (3)$$

Interpolation in the f-tables is performed as a quadratic function of the square root of the fuel temperature, $\sqrt{T_f}$, and the logarithm of the microscopic background cross section, $\log(\sigma_0)$. Self-shielded data for each resonance absorber are generated at different temperatures and at different background cross section conditions between 10 barns and 10^{10} barns (i.e., infinitely dilute).

2.2. Obtaining Effective Resonance Data from the Cross Section Library

2.2.1. Calculation of Background Cross Sections

In order to use the resonance data contained in the cross section library, the f-tables must be entered with the proper microscopic background cross section for each isotope in each fuel mixture. The task, then, is to calculate an accurate value of the microscopic background cross section.

The microscopic background cross section for any particular isotope, $\sigma_{0,iso}$, is obtained from the macroscopic background cross section for the fuel mixture as a whole, Σ_0, using the relationship,

$$\sigma_{0,iso} = \frac{\Sigma_0}{N_{iso}} - \sigma_{p,iso} \tag{4}$$

where N_{iso} is the number density of isotope *iso*; and $\sigma_{p,iso}$ is the microscopic potential scattering cross section for isotope *iso*.

The calculation of a macroscopic background cross section for an isolated fuel pin is separated into two components: (1) a volume component (potential scattering), Σ_p; and (2) a surface component (escape), Σ_e. The macroscopic background cross section is the sum of the two components, $\Sigma_0 = \Sigma_p + \Sigma_e$ [3].

The volume component accounts for neutrons that are scattered into an energy resonance by the fuel material and is expressed as the sum of the potential scattering cross sections for all isotopes in the fuel mixture,

$$\Sigma_p = \sum_{iso} N_{iso} \sigma_{p,iso} \tag{5}$$

The potential scattering cross section is energy-independent and represents the forces that act upon a neutron as it moves in or near the nucleus. It is a function only of the effective scattering radius of the nucleus, which depends on the way in which the different wavelengths of the incident neutron (e.g., s-wave, p-wave, etc.) interact with the target nucleus. The effective scattering radius of each isotope is obtained from the ENDF/B files and the potential scattering cross section is then calculated as,

$$\sigma_{p,iso} = 4\pi R_{0,iso}^2 \tag{6}$$

where $R_{0,iso}$ is the effective scattering radius of the nuclide.

The surface component of the macroscopic background cross section accounts for neutrons that escape the fuel pellet and are scattered into an energy resonance by the surrounding moderator. The neutrons then have a finite probability of re-entering the fuel pellet and being absorbed. The surface component for an isolated fuel pellet can be approximated using the Wigner rational expression [4], where the macroscopic escape cross section, Σ_e, is expressed as the inverse of the mean chord length for a simple convex body,

$$\Sigma_e = \left(\frac{4V}{S} \right)^{-1} = \frac{1}{2r} \tag{7}$$

where V refers to the volume of the fuel pellet; S refers to the pellet surface area; and r is the pellet radius. In this case, the 'fuel pellet' has been smeared across the pellet/cladding gap, and the geometric volume, surface area, and the pellet radius therefore correspond to the inner cladding radius. The mean chord length for a pellet subdivided into multiple annular rings is calculated following the method outlined in [5].

The Wigner rational expression is an excellent approximation for certain applications; however it has its limitations. For typical LWR analysis, errors in the Wigner rational expression can lead one to enter the pre-processed resonance tables in the wrong location. For such applications, the Wigner approximation is augmented with a Bell factor [3] (denoted *a*) to produce more acceptable results. This leads to the macroscopic escape cross section for an isolated rod,

$$\Sigma_e^{isolated} = a\left(\frac{4V}{S}\right)^{-1} = \frac{a}{2r} \tag{8}$$

The LANCR02 Bell factor is a sensitive function mildly dependent on fuel temperatures and pellet radii, centered on values that are typical to a Light Water Reactor. Although the adjusted Bell factor is relatively close to the Bell recommended value (e.g. 1.16, ref. [3]), it provides flexibility for customization to LWR fuel lattice and temperature conditions.

[[

]]

[[

]]

Figure 2-1 Comparison of the escape probability approximated with a Bell factor to a two-term Carlvik Rational Approximation

[[

]]

2.2.2. Dancoff Factors

The Wigner rational expression in Eq. (8) is applicable only to an isolated fuel pellet. For an array of tightly packed fuel pins, some neutrons may escape from one pellet and suffer their first collision in a neighboring pellet rather than in the surrounding moderator. This shadowing effect will alter the Wigner rational expression from that for an isolated fuel pin and is taken into account through the use of a Dancoff factor, Γ. The Dancoff factor is calculated using Sugimura and Yamamoto's neutron current method [6] and applied to the

escape cross section. The new expression for the macroscopic background cross section becomes,

$$\Sigma_0 = \Sigma_p + \Gamma\Sigma_e^{isolated} \tag{9}$$

In the neutron current method, Dancoff factors are evaluated using flux values obtained from two separate solutions. The first solution is a fixed source calculation on the entire lattice in the bundle's true geometry. The second solution is a fixed source calculation on an isolated pin cell. The isolated pin cell problem supplies the reference flux for an unshielded fuel pin. The lattice calculation supplies the shielded flux for each pin location in the bundle.

The Dancoff factor can be expressed in terms of the Dancoff correction, C,

$$\Gamma = 1 - C \tag{10}$$

The Dancoff correction is defined in terms of the number of neutrons that enter the surface of the fuel pin from the moderator region. For an isolated fuel pin with a fixed source of neutrons in the moderator region, the number of neutrons entering the surface of the pin can be represented as I_0. For fuel pins in a bundle, the neighboring fuel pins will shield each other to some extent and the number of neutrons entering the pin surface can be represented by I, which will be somewhat smaller than I_0. The definition of the Dancoff correction is calculated as the ratio of the two surface currents,

$$C = \frac{I_0 - I}{I_0} \tag{11}$$

If it is assumed that the fuel pins are entirely black to all resonance neutrons (i.e., all neutrons that reach the fuel pin are absorbed), then the surface currents are then independent of the moderator source intensity and the Dancoff correction can be expressed in terms of the flux in the fuel pins rather than the surface currents,

$$C = \frac{\phi_0 - \phi}{\phi_0} \tag{12}$$

The fluxes in Eq. (12) are solved using the MoC transport module, which is described in Section 3 of this report. The transport solver is called twice – once to perform a fixed source calculation on the entire lattice, and once to perform a fixed source calculation on an isolated fuel pin. In both calculations, fixed sources are placed in all regions of the problem other than the fuel regions. The sources are normalized such that $S/\Sigma = \gamma$, where S is the source strength in a region of the problem; Σ is the total cross section in the region; and γ is an arbitrary constant. For such a definition, the sources in each region of the problem will be given by $S = \gamma \cdot \Sigma$, where the constant is totally arbitrary and is uniform over the entire problem domain. After performing both fixed-source calculations, Dancoff corrections for every fuel pin location are calculated using Eq. (12) and the corresponding Dancoff factor for

each pin location in the lattice is calculated using Eq. (10). If the lattice contains fuel rods of different dimensions, then the isolated pin cell calculation is performed once for each unique rod.

[[

]]

2.2.3. Final Background Cross Sections

For each isotope in the fuel mixture, the associated microscopic background cross section is calculated using Eqs. (4) and (9). The microscopic background cross section is then used to enter the resonance tables and obtain the appropriate cross sections for each resonance absorber isotope in each fuel mixture in the lattice.

The method described in this sub-section is a simple technique for obtaining background cross sections. Nevertheless, with an appropriate value of the Bell factor, this simple technique used in LANCR02 is very accurate for BWR applications and produces cross sections in the resonance energy range that are in good agreement with cross sections created from MCNP reference solutions.

2.3. Energy Condensation

Once microscopic cross sections have been obtained from the cross section library and the macroscopic cross sections have been created for each material region in the lattice, the flux distribution can be determined. The LANCR02 methodology supports the solution of the Boltzmann transport equation in the fine-group energy structure, but the calculation is very time consuming and does not necessarily yield a significant benefit in accuracy.

A reduction in the solution can be obtained by condensation of the macroscopic cross sections from the fine-group energy structure (e.g. 118 groups) to a more manageable smaller transport energy group structure (e.g. 23 groups),

$$\Sigma_{x,i}^{G} = \frac{\sum_{g \in G} \Sigma_{x,i}^{g} \tilde{\phi}_{i}^{g}}{\sum_{g \in G} \tilde{\phi}_{i}^{g}} \tag{13}$$

where $\Sigma_{x,i}^{G}$ and $\Sigma_{x,i}^{g}$ are the macroscopic cross sections of reaction x for the transport group (superscript G) and fine-group (superscript g) structures, respectively. The weighting function

$\tilde{\phi}_i^g$ is an approximation to the flux in region *i* generated by a two-step process that consists of a series of one-dimensional pin cell calculations followed by a fast two-dimensional coupling calculation. Both calculations are performed in the fine-group energy structure of the LANCR02 cross section library. Although the two step-method does not necessarily produce accurate flux solution, it will give accurate relative fine-group fluxes which can be used as weighting functions for the condensation. This sub-section is used to describe the methodology behind the condensation scheme.

2.3.1. One-Dimensional Pin Cell Spectral Calculations

Each pin cell in the lattice – including water rods and empty cells (i.e., vanish locations) - takes part in its own unique one-dimensional pin cell spectral calculation. The flux in the system is determined by solving the integral form of the transport equation using the method of collision probabilities (CP) [11], [12]. The CP method is ideal for physically small systems containing a small number of material regions and a limited number of mesh. For each pin cell calculation, the square coolant region of each cell is cylindricalized by preserving volume. A buffer zone, made up of lattice-averaged fuel and moderator material, is added to the outside of each cell to help drive the flux across inert pins and pins containing strong absorbers (e.g., gadolinium), as illustrated in Figure 2-2. The pin cell system is represented as a fixed source problem, where the fission spectrum is used as the neutron source and is placed only in the buffer zone. This helps to facilitate a speedy convergence to the transport solution without affecting the final flux spectrum.

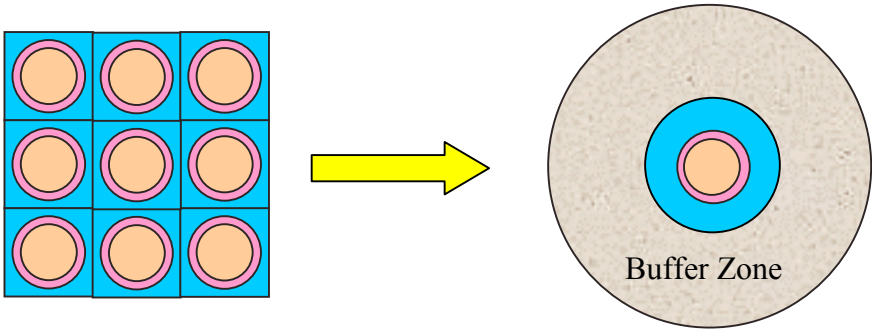

Figure 2-2 Geometry of a pin cell with a buffer zone attached to the outside

The scalar flux is determined by solving the following integral equation,

$$\phi(\vec{r}_i, E) = \int_V Q(\vec{r}_j, E) \cdot T(\vec{r}_j \rightarrow \vec{r}_i, E) \cdot dV_j \qquad (14)$$

where $Q(\vec{r}_j, E)$ is the neutron source in mesh *j*; and $T(\vec{r}_j \rightarrow \vec{r}_i, E)$ is the first-flight transmission probability (i.e., flux contribution) of neutrons from mesh *j* to mesh *i*, given by the expression,

$$T(\vec{r}_j \rightarrow \vec{r}_i, E) = \frac{e^{-\tau(\vec{r}_i - \vec{r}_j, E)}}{4\pi \left| \vec{r}_i - \vec{r}_j \right|^2} \tag{15}$$

Here $\tau(\vec{r}_i - \vec{r}_j, E) = \int_0^{\left|\vec{r}_i - \vec{r}_j\right|} \Sigma_t(\vec{r}_i - \vec{\Omega}s, E) \cdot ds$ is the optical path between mesh *j* and mesh *i* in the neutron's direction, $\vec{\Omega}$.

In order to arrive at the expression for the scalar flux in Eq. (14), the source term is assumed to be constant across a mesh (i.e., flat flux/flat source approximation) and isotropically distributed in angle. The assumption of an isotropic source requires the use of transport-corrected cross sections in order to account for anisotropic scattering effects. To arrive at the transport-correction, the flux is expanded using Legendre polynomials and the first two terms from the resulting expression are used in the spherical harmonics form of the transport equation. This leads to the diffusion equations for the scalar flux, ϕ^g, and current, J_1^g, and the corresponding definition for the diffusion coefficient,

$$D^g = \frac{1/3}{\Sigma_{t_1}^g - \sum \Sigma_{s_1}^{g' \rightarrow g} \left(J^{g'} / J^g \right)} \tag{16}$$

The denominator in Eq. (16) is the definition for the transport cross section, which is a function of the ratio of currents in various energy groups. Since the currents are not known *a priori*, the current-induced scattering of neutrons into an energy group is assumed to be approximately equal to the current-induced scattering of neutrons out of the energy group,

$$\sum_{g'} \Sigma_{s_1}^{g' \rightarrow g} J^{g'} \approx \sum_{g'} \Sigma_{s_1}^{g \rightarrow g'} J^g \tag{17}$$

This is a fair assumption when scattering is the dominant process and relatively little neutron absorption is taking place. It is a poor assumption when absorption is the dominant process, such as in a control blade or a fuel pin containing gadolinium.

From Eq. (17) it follows that,

$$\Sigma_{tr}^g = \Sigma_t^g - \sum_{g'} \Sigma_{s_1}^{g \rightarrow g'} = \Sigma_t^g - \Sigma_{s_1}^g \tag{18}$$

which is the LANCR02 definition for the transport cross section and, hence, the transport-correction. In Eq. (18), Σ_t^g is the total cross section in group g; and $\Sigma_{s_1}^g$ is the first moment of the total scattering cross section in group g (i.e., $\Sigma_{s_1}^g = \bar{\mu}^g \Sigma_{s_0}^g$).

In a one-dimensional cylindrical geometry, the neutron motion in the polar direction is eliminated by assuming an isotropic source and integrating the flux over z. The transmission kernel then relies only on the optical distances in the plane of the problem,

$$T_{i\leftarrow j}^{g} = \frac{P_{i\leftarrow j}^{g}}{\Sigma_i^g V_i}$$

$$\Sigma_i^g V_i P_{i\leftarrow j}^{g} = \frac{1}{2\pi}\int d\varphi \int dy [Ki_3(\tau_{ij}^g) - Ki_3(\tau_{ij}^g + \tau_j^g) - Ki_3(\tau_{ij}^g + \tau_i^g) + Ki_3(\tau_{ij}^g + \tau_j^g + \tau_i^g)] \quad (19)$$

where $Ki_3(\tau)$ are Bickley-Nayler functions that account for the motion of neutrons out of the plane of the problem. All CP's originating from each mesh are normalized to enforce neutron conservation. That is, a neutron born within a mesh must have a total probability equal to 1.0 of having a collision somewhere.

Specular reflection boundary conditions are used on the outside of the one-dimensional pin cell geometry to simulate perfect reflection in the square moderator system (i.e., Weigner-Seitz cell). This is accomplished using Carlvik's modification to the black boundary collision probabilities,

$$\Sigma_{tr,i}^g V_i \hat{P}_{i\leftarrow j}^{g} = \Sigma_{tr,i}^g V_i P_{i\leftarrow j}^{g} + \frac{R_j R_i}{\sum_j R_j} \quad (20)$$

where $R_i^g = \Sigma_{tr,i}^g V_i - \sum_j \Sigma_{tr,j}^g V_j P_{i\leftarrow j}^{g}$ [12]. The white boundary collision probabilities, $\hat{P}_{i\leftarrow j}^{g}$, are used in Eq. (19) in place of the black boundary collision probabilities, $P_{i\leftarrow j}^{g}$.

The integrations in Eq. (19) are performed numerically using sets of parallel, equidistant tracks (spaced a distance *dy* apart), which are traced over the geometry of the system at several equally spaced azimuthal angles (distributed every $d\varphi$ radians). The collision probabilities between the various mesh and boundaries are then calculated along these tracks. In one-dimensional cylindrical geometry, the integration over angle is contained within the spatial integration, as illustrated in Figure 2-3, and only a single set of tracks needs to be traced over the system.

Expressing the multi-group equations of the CP method as a coupled system of linear equations,

$$\phi_i^g = \sum_j T_{i\leftarrow j}^g S_j^g + \sum_j T_{i\leftarrow j}^g V_j \Sigma_{s_j}^{g\leftarrow g} \phi_j^g$$

$$S_j^g = \sum_{g'\neq g} V_j \Sigma_{s_j}^{g\leftarrow g'} \phi_j^{g'} + F_j^g$$

$$\sum_j \phi_j^g (\delta_{i,j} - \Sigma_{s_j}^{g \leftarrow g} T_{i \leftarrow j}^g V_j) = \sum_j T_{i \leftarrow j}^g S_j^g \tag{21}$$

where F_j^g is the fixed source in region j. The system in Eq. (21) can be expressed in matrix form as,

$$\underline{\underline{A}}\,\underline{\phi} = \underline{B} \tag{22}$$

where the matrix elements are defined as,

$$a_{ij}^g = \delta_{ij} - \Sigma_{s_j}^{g \leftarrow g} T_{i \leftarrow j}^g V_j$$
$$b_i^g = \sum_j T_{i \leftarrow j}^g S_j^g$$

Solution to Eq. (22) is obtained from $\underline{\phi} = \underline{\underline{A}}^{-1}\underline{B}$, where $\underline{\underline{A}}^{-1}$ is the inversion of $\underline{\underline{A}}$, performed by Gauss-Jordan elimination before beginning the flux iterates.

The solution to Eq. (22) yields a flux spectrum in each region of each pin cell in the fine-group energy structure of the cross section library. Even though each pin cell geometry contains an outer buffer zone, the flux has been generated without considering the effects of the true surroundings on the spectrum (e.g., the effects of water gaps, water rods, strong absorber pins, control blades, etc.).

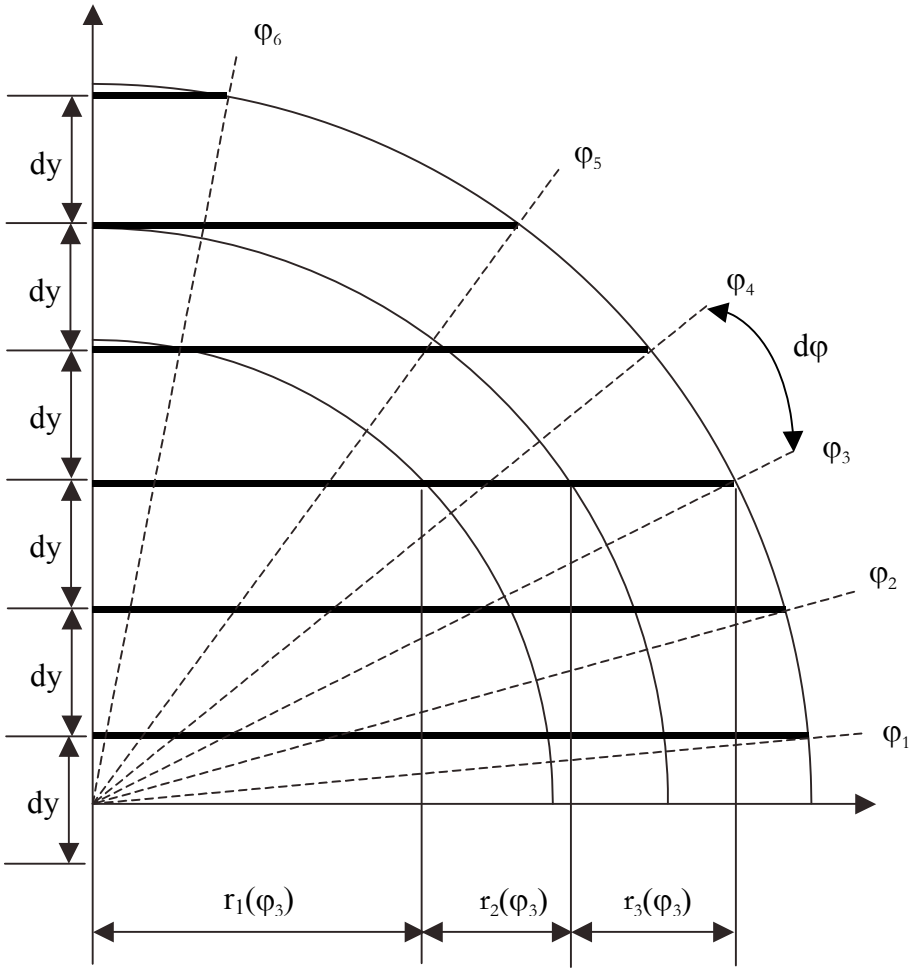

Figure 2-3 Integration variables associated with cylindrical geometry.

2.3.2. Two-Dimensional Coupling Calculation

Before condensing cross sections to smaller transport energy group structure, the spectrums from the one-dimensional pin cell calculations need to be updated to account for the effects of the true surroundings. In LANCR02, this is accomplished by performing a two-dimensional calculation on the entire lattice using a simplified geometry and a simplified solution to the transport equation.

The two-dimensional coupling calculation solves the integral transport equation using a response matrix (RM) method based on simplified transmission kernels [13]. Each pin cell is homogenized into an equivalent material set of cross sections using the fluxes from the 1-D pin cell calculations. Cells are coupled to each other via surface currents, which are assumed to be isotropically distributed. For an accurate solution to the transport equation, such assumptions would not be possible. However, for the purpose of generating a condensation spectrum, such assumptions are acceptable.

The equations representing the scalar flux and outward-directed currents are, respectively,

$$\phi_I^g = T_{I\leftarrow I}^g Q_I^g V_I + \sum_s T_{I\leftarrow s}^g J_{s,in}^g A_s \tag{23}$$

$$J_{s,out}^g = T_{s\leftarrow I}^g Q_I^g V_I + \sum_{s'} T_{s\leftarrow s'}^g J_{s',in}^g A_{s'} \tag{24}$$

where I represents a spatial mesh, such as a homogenized pin cell; s represents a surface to mesh *I*; the *T*'s are transmission kernels between volumes and/or surfaces; *V* represents the volume of mesh *I*; and A_s represents the surface area of surface s. Outward-directed currents from one mesh become the inward-directed currents to the neighboring mesh.

Transmission kernels are calculated by tracing streaming rays at different angles, dφ, over each individual mesh in the problem, along which the integrations to the TP expressions are performed, as illustrated in Figure 2-4. The volume-to-volume, surface-to-volume, and surface-to-surface transmission kernels are calculated as,

$$T_{i\leftarrow i}^g = \frac{1}{\Sigma_{tr_i}^g V_i} \int \frac{d\varphi}{2\pi} \int dy \cdot P_{i\leftarrow i}^g$$

$$T_{i\leftarrow s}^g = \frac{1}{\Sigma_{tr_i}^g V_i} \int \frac{d\varphi}{2\pi} \int dy \cdot P_{i\leftarrow s}^g$$

$$T_{s\leftarrow s'}^g = \frac{2}{A_{s'}} \int \frac{d\varphi}{2\pi} \int dy \cdot P_{s\leftarrow s'}^g \tag{25}$$

where the collision probabilities are expressed in terms of Bickley-Nayler functions, $Ki_3(\tau)$, just as in the CP method,

$$P_{i\leftarrow i}^g = 1 - \frac{1}{\Sigma_{tr_i}^g V_i}\left[\frac{\pi}{4} - Ki_3(\tau_{i\leftarrow i}^g)\right]$$

$$P_{i\leftarrow s}^g = \frac{1}{2A_s}\left[\frac{\pi}{4} - Ki_3(\tau_{i\leftarrow s}^g)\right]$$

$$P_{s\leftarrow s'}^g = \frac{1}{2A_{s'}} Ki_3(\tau_{s\leftarrow s'}^g) \tag{26}$$

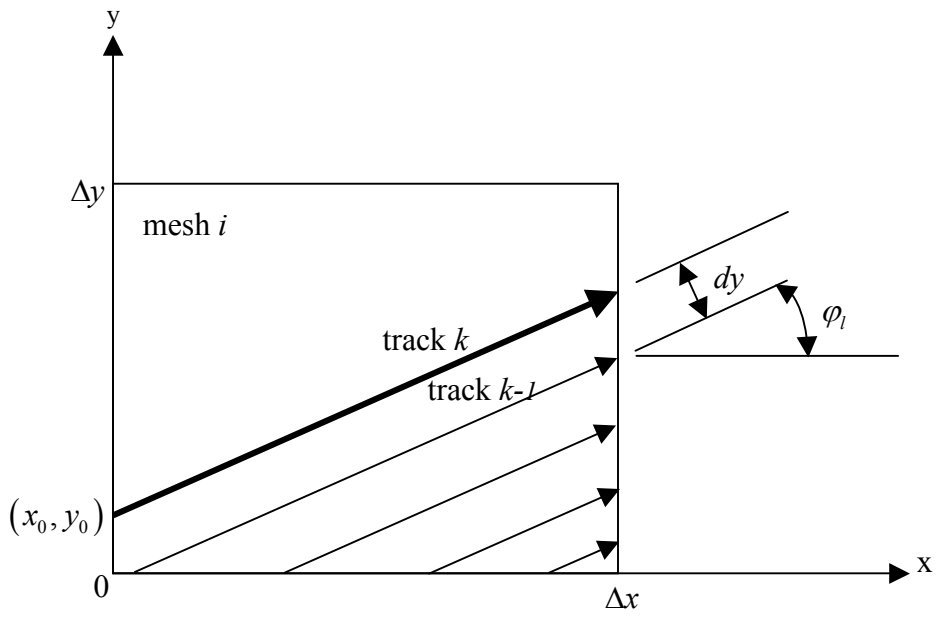

Figure 2-4 Streaming rays traced across a mesh at a specific angle

The CP's that originate from each mesh are normalized to enforce neutron conservation, just as is done for the pin cell calculations.

In Eq. (26), the τ's are optical distances between volumes and/or surfaces in the xy-plane of the problem. Fluxes and currents are solved using a red-black iteration scheme.

Following the completion of the coupling calculation, the energy distribution of neutrons from the 1-D pin cell calculations are updated to account for the effects of the surroundings,

$$\tilde{\phi}_i^g = \phi_i^g \cdot \frac{\phi_I^g V_I}{\sum_{i \in I} \phi_i^g V_i} \tag{27}$$

where *i* is each region within pin cell *I*.

Fluxes for the surrounding regions of the lattice – channel box wall and water gaps – are obtained directly from the RM solution. Fluxes for the various regions of a control blade are obtained from a series of one-dimensional pin cell calculations performed on each absorber tube in a control blade and updated with the flux from the RM solution. Eq. (27) represents the flux for each material region of the problem that will be used to condense the macroscopic cross sections. The final energy group structure for the two-dimensional transport calculation depends on the accuracy of the condensation scheme, the energy group boundaries in the original fine-group energy structure of the cross section library, and the types of problems to be analyzed by the lattice physics code.

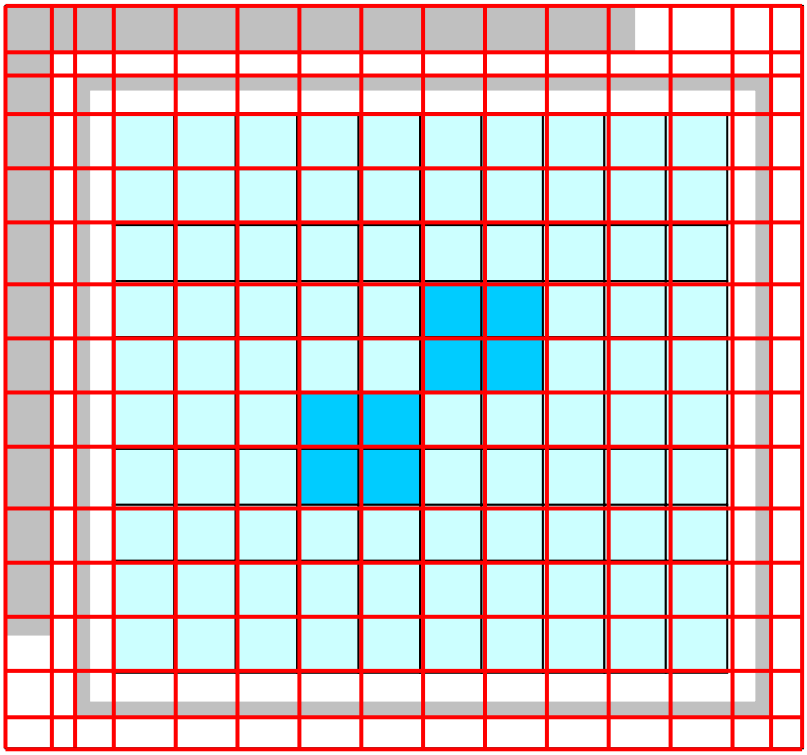

Figure 2-5 Typical geometry of coupling calculation for a 10x10 lattice with control blade

2.4. Two-Dimensional Transport Calculation

After performing the RM calculation and collapsing the cross sections to the transport group structure, the final two-dimensional lattice calculation is performed by solving the Boltzmann transport equation, using the Method of Characteristics (MoC) [10], [14]. The multi-group, discrete angle Boltzmann equation with isotropic scattering of the form,

$$\Omega_m \cdot \nabla \Phi_i^g(\Omega_m) + \Sigma_{tr,i}^g \Phi_i^g(\Omega_m) = \frac{1}{4\pi}\left[\sum_{g'} \Sigma_{s,i}^{g' \to g} \phi_i^{g'} + \frac{\chi^g}{k} \sum_{g'} \nu \Sigma_{f,i}^{g'} \phi_i^{g'}\right] \tag{28}$$

then can be expressed as,

$$\frac{d\Phi_{m,i}^G}{ds_m} + \Sigma_{tr,i}^G \Phi_{m,i}^G = Q_{m,i}^G \tag{29}$$

where s_m is the length along a streaming track across a mesh at angle Ω_m, $\Phi_{m,i}^G$ is the angular flux in direction Ω_m, across mesh *i*, in energy group *G*; and $Q_{m,i}^G$ is the corresponding angular source, which is calculated using transport-corrected cross sections.

To solve the Characteristics equation (29), streaming tracks are traced over the problem geometry at a number of different angles. Each angle has associated with it a weight, and each track has associated with it a width. Solution to the Characteristics equation, in terms of the angular flux, is obtained along streaming rays and is of the form,

$$\Phi_{m,i}^{G}(s_m) = \Phi_{m,i}^{G}(0)e^{-\Sigma_{tr,i}^{G}s_m} + \frac{Q_{m,i}^{G}}{\Sigma_{tr,i}^{G}}(1-e^{-\Sigma_{tr,i}^{G}s_m}) \tag{30}$$

where the source across a mesh is considered constant (i.e., flat source/flat flux approximation).

The scalar flux for a given mesh is calculated by integrating the angular flux along all streaming tracks that cross the mesh, and integrating over all directions of motion,

$$\phi_i^G = \int_{4\pi} \bar{\Phi}_i^G(\Omega)d\Omega = 4\pi\sum_m \bar{\Phi}_{m,i}^G\omega_m \tag{31}$$

where ω_m is the weight associated with each direction of motion; and $\bar{\Phi}_{m,i}^G$ is the average angular flux in a specific direction across a given mesh, calculated as,

$$\bar{\Phi}_{m,i}^G = \frac{\sum_k \bar{\Phi}_{m,k,i}^G \cdot s_{m,k,i} \cdot d_m}{\sum_k s_{m,k,i} \cdot d_m} \tag{32}$$

where d_m is the separation between parallel streaming tracks; $s_{m,k,i}$ is the length of the streaming track crossing mesh *i*; and *k* represents the different streaming tracks that cross mesh *i* in direction Ω_m. To obtain an expression for the average value of the angular flux along a streaming track, $\bar{\Phi}_{m,k,i}^G$, Eq.(30) is integrated along the track of motion and divided by the length of the track,

$$\bar{\Phi}_{m,k,i}^G = \frac{\int_0^{s_{m,k,i}} \Phi_{m,k,i}^G(s')ds'}{\int_0^{s_{m,k,i}} ds'} \tag{33}$$

Solution to the characteristics equation reduces to finding the intersections between rays and mesh boundaries and calculating the angular flux between intersections. The final solution to the equation produces a very detailed flux distribution throughout the lattice in the condensed transport energy group structure.

Section 3 of this report presents a much more detailed description of the MoC technique as implemented in LANCR02**.**

2.5. Fundamental Mode Calculation

The MoC lattice calculation assumes perfect reflection on all surfaces of the bundle. In this way, there are no neutrons leaking into or out of the system. However, the data that is generated by the lattice physics code will be used in a nodal code to model an entire reactor and, within the reactor, there are almost always neutrons leaking into or out of each node in the system. To be consistent with the way in which the nodal cross sections are to be used, LANCR02 must somehow account for neutron leakage at the lattice physics level.

Leakage effects are included in an *ad hoc* way by performing a buckling calculation on the lattice to find the leakage/buckling (in or out) that will make the lattice critical (k_{eff}=1). LANCR02 solves the fundamental mode equation in the diffusion approximation for an energy-independent material buckling,

$$\bar{\Sigma}_r^g \Psi^g + B_m^2 \bar{D}^g \Psi^g = \sum_{g' \neq g} \bar{\Sigma}_s^{g \leftarrow g'} \Psi^{g'} + \bar{\chi}^g \tag{34}$$

where $\bar{D}^g = 1/\left(3\bar{\Sigma}_{tr}^g\right)$ is the lattice-averaged diffusion coefficient, $\bar{\Sigma}_r^g = \bar{\Sigma}_{tr}^g - \bar{\Sigma}_s^{g \leftarrow g}$ is the lattice-averaged removal cross section, and Ψ^g is the leakage adjusted fundamental mode flux.

Eq. (34) assumes that the flux has been normalized to a single neutron being lost from the system, $\sum_g (\bar{\Sigma}_a^g + \bar{D}^g B_m^2)\Psi^g = 1$. The eigenvalue in the system is then calculated from,

$$k_{eff} = \sum_g \nu \bar{\Sigma}_f^g \Psi^g \tag{35}$$

B_m^2 is adjusted until k_{eff}=1. The value of the buckling will be positive if the initial lattice eigenvalue was greater than unity, and the buckling will be negative if the initial lattice eigenvalue was less than unity.

The fundamental mode calculation is performed in the fine-group energy structure of the cross section library. This more accurately captures the leakage effects in the fast energy range, where the mean-free-paths are longer and most neutron leakage occurs. The fine-group flux is determined by:

$$\phi_i'^g = \tilde{\phi}_i^g \cdot \frac{\phi_i^G}{\sum_{g \in G} \tilde{\phi}_i^g} \tag{36}$$

where $\tilde{\phi}_i^g$ is the fine-group condensation flux from Eq. (27); and ϕ_i^G is the transport-group flux from the MoC calculation, given by Eq. (31).

After expanding the MoC flux, the lattice-averaged cross sections are calculated by volume- and flux-weighting the individual cross sections from the various regions of the problem,

$$\overline{\Sigma}_x^g = \frac{\sum_i \Sigma_{x,i}^g \phi_i'^g V_i}{\sum_i \phi_i'^g V_i} \tag{37}$$

In Eq. (37), x is a reaction type and $\phi_i'^g$ is the MoC flux distribution after being expanded back to the fine-group energy structure.

To perform the buckling search, an initial calculation is performed by setting $B_m^2 = 0$. This reproduces the infinite lattice eigenvalue. A second calculation is performed by setting the buckling to a very small positive value, e.g., $B_m^2 = 10^{-6}$. The eigenvalues from the first two calculations are used to extrapolate the buckling value to a new value and the corresponding eigenvalue is calculated using Eq. (35). This process continues until an eigenvalue sufficiently close to unity is obtained (i.e., $\left|k_{eff} - 1\right| < \varepsilon$). This produces the flux spectrum for a critical system and the expanded flux distribution from the MoC solution is adjusted to account for leakage effects,

$$\phi_i''^g = \phi_i'^g \cdot \frac{\Psi^g \cdot \sum_i V_i}{\sum_i \phi_i'^g V_i} \tag{38}$$

Eq. (38) represents the final flux distribution for the lattice. The leakage flux is used to create the nodal data and to deplete the burnable isotopes in the fuel.

The adjoint flux is also needed to accurately generate nodal kinetics data for the effective delayed neutron fraction, β_{eff}^j, and the prompt neutron lifetime, l_p,

$$\begin{aligned}\beta_{eff}^j &= \frac{\sum_{iso}\left[\beta_{iso}^j\left(\sum_g \overline{\chi}_{d,iso}^{g,j}\Psi^{\dagger g}\right)\left(\sum_g \nu\overline{\sigma}_{f,iso}^g \overline{N}_{iso}\Psi^g\right)\right]}{\sum_{iso}\left[\left\{\left(1-\sum_{i=1}^6 \beta_{iso}^i\right)\cdot\sum_g \overline{\chi}_p^g\Psi^{\dagger g} + \sum_{i=1}^6\left(\beta_{iso}^i\left(\sum_g \overline{\chi}_{d,iso}^{g,i}\Psi^{\dagger g}\right)\right)\right\}\left\{\sum_g \nu\overline{\Sigma}_{f,iso}^g\Psi^g\right\}\right]} \\ &= \frac{\sum_{iso}\left[\beta_{iso}^j\left(\sum_g \overline{\chi}_{d,iso}^{g,j}\Psi^{\dagger g}\right)\left(\sum_g \nu\overline{\sigma}_{f,iso}^g \overline{N}_{iso}\Psi^g\right)\right]}{\sum_g \overline{\chi}^g\Psi^{\dagger g}\cdot\sum_g \nu\overline{\Sigma}_f^g\Psi^g}\end{aligned} \tag{39}$$

$$l_p = \frac{\sum_g \frac{1}{v^g}\Psi^{\dagger g}\Psi^g}{\sum_g \overline{\chi}^g\Psi^{\dagger g}\cdot\sum_g \nu\overline{\Sigma}_f^g\Psi^g} \tag{40}$$

where the outer summation in Eq. (39) is over major actinides in the fuel and j represents a delayed neutron group. The adjoint flux is approximated by solving the adjoint to the fundamental mode equation,

$$\overline{\Sigma}_r^g \Psi^{+g} = \sum_{g' \neq g} \overline{\Sigma}_s^{g \to g'} \Psi^{+g'} + \nu \overline{\Sigma}_f^g \sum_{g'} \chi^{g'} \Psi^{+g'} \tag{41}$$

where the removal cross section now contains the leakage term, $\overline{\Sigma}_r^g = \overline{\Sigma}_{tr}^g - \overline{\Sigma}_s^{g \leftarrow g} + B_m^2 \overline{D}^g$. In this derivation, the spatial component of the adjoint flux is assumed to be equivalent to the spatial component of the forward flux and only the energy distribution of the adjoint flux is assumed to differ from that of the forward flux.

In addition to the leakage corrected adjoint solution calculated above it is also possible to solve for the infinite adjoint flux in Eq. (41) by omitting the leakage term from the removal cross section.

2.6. Gamma Transport Calculation

The LANCR02 methodology includes an explicit gamma transport calculation that provides a detailed rod-by-rod gamma energy deposition edit, along with a gamma detector response for a detector present in the SE corner of the lattice. The gamma calculation is performed using the same MoC module as is used to solve the neutron eigenvalue problem. Steady state gamma sources are calculated for each region of the lattice in a gamma energy group structure. The gamma calculation is a fixed source calculation that uses cross sections from a gamma library, where the gamma sources, due to neutron capture and fission, are given by the following expressions,

$$q_{capture}^{\gamma} = \sum_G N_{iso} \sigma_{capture,iso}^G V_i \phi_i^G q_{capture,iso}^{\prime G} \chi_{capture,iso}^{G \to \gamma} \tag{42}$$

$$q_{fission}^{\gamma} = \chi_{fission,iso}^{\gamma} \cdot q_{fission,iso}^{\prime} \sum_G N_{iso} \sigma_{fission,iso}^G V_i \phi_i^G \tag{43}$$

Here, $q_{capture,iso}^{\prime G}$ is the gamma energy (in MeV/fission) released by neutron capture in isotope iso, neutron energy group G; $q_{fission,iso}^{\prime}$ is the total gamma energy (in MeV/fission) released through neutron fission in isotope iso; $\chi_{capture,iso}^{G \to \gamma}$ is the gamma spectrum that distributes the energy released from neutron capture in neutron energy group G, isotope *iso*, to gamma energy group γ; and $\chi_{fission,iso}^{\gamma}$ is the gamma spectrum that distributes the energy released from fission in isotope *iso*. Fission gamma sources include both delayed and prompt gamma emission. The total fixed source in each region of the problem is the sum of Eq. (42) and Eq. (43).

The LANCR02 gamma transport methodology uses the same geometry and angular detail to solve the MoC equation as is used to determine the neutron flux distribution. The total fixed source per mesh for the MoC equation is given by,

$$q_n^\gamma = q_{capture,n}^\gamma + q_{fission,n}^\gamma + \sum_{\gamma'} \Sigma_{s,n}^{\gamma' \to \gamma} \phi_n^{\gamma'} \tag{44}$$

2.6.1. Calculation of Local Gamma Energy Deposition

Gamma energy deposition in each unique material region of the lattice is calculated by using the converged gamma fluxes and macroscopic energy deposition cross sections,

$$E_{\gamma,i} = \sum_{\gamma} \Sigma_{e,i}^{\gamma} V_i \phi_i^{\gamma} \tag{45}$$

where $\Sigma_{e,i}^{\gamma}$ is the gamma energy deposition cross section that is read from the gamma cross section library.

Eq. (45) is solved for each fuel rod individually and for other material regions as a whole. Edits are supplied for the rod-by-rod gamma energy distribution and for the energy deposited in the coolant, cladding, channel box wall, bypass region, water rods, and control blade. These edits do not include other forms of energy deposition, such as conduction through the channel wall or kinetic heating from neutron slowing down in the coolant.

2.6.2. Calculation of Gamma Detector Response

The detector response is currently defined as the energy deposited to the detector in Watts at the assembly average power density level defined via input. The energy deposition cross section for the detector is obtained from iron (Fe). The equation for calculating the gamma J-factor is described in Section 8 of this report.

3. DETAILS OF THE CHARACTERISTICS MODULE

Subsection 2.4 presented a very brief overview of the basic equations solved when implementing the MoC technique. This section will be used to describe the MoC implementation in LANCR02 in more detail. The characteristics solution has become a popular choice for lattice physics applications, and this section is used to give the reader a deeper understanding of the method that forms the foundation of the LANCR02 lattice physics.

3.1. Quadrature Set

In order to model neutron motion in the MoC technique, streaming rays (i.e., characteristics) are traced across the two-dimensional system in a number of different directions, where the accuracy of the solution depends on the total number of directions modeled and the spacing between parallel rays. The discrete directions of motion are defined using a quadrature set [15], which consists of a set of azimuthal angles and a separate set of polar angles, as illustrated in Figure 3-1. Directions of motion pass through the centroid of the solid angle subtended by the boundaries on a unit sphere. The weight associated with each direction of motion is equal to the area of the solid angle.

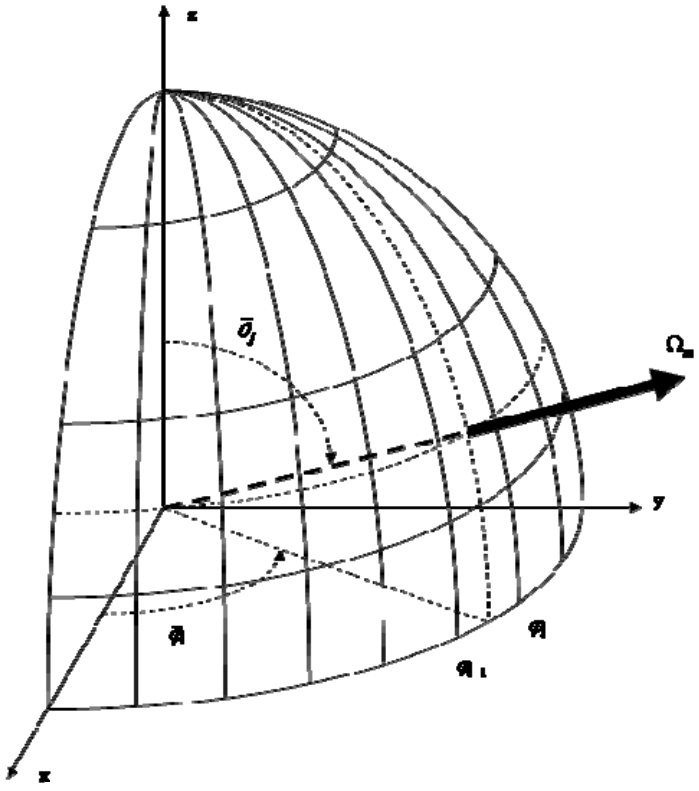

Figure 3-1 Example of a quadrature for the MoC.

3.1.1. Azimuthal Angles of Motion

The azimuthal angles of motion for LWR applications are evenly spaced in the xy-plane of the problem. For a specified number of azimuthal directions, N_a, the boundaries of motion are spaced at intervals $\Delta\varphi = 2\pi/N_a$ apart and the azimuthal direction of motion takes place through the center of two neighboring boundaries,

$$\bar{\varphi}_i = \frac{1}{2}(\varphi_{i-1} + \varphi_i) \tag{46}$$

where $\varphi_0 = 0$. The weight associated with each azimuthal direction of motion is equal to the area between the boundaries, $\omega_i = 2\pi/N_a$. The total weight of all azimuthal directions sums to 2π.

[[

]]

3.1.2. Polar Angles of Motion

The polar directions of motion are distributed using the Tabuchi-Yamamoto optimal quadrature set [15]. The code also contains several Legendre quadrature sets that can be chosen by the user via input parameters. There are 3 separate optimal quadrature sets and six separate Legendre quadrature sets to choose from in the MoC module. The optimal quadrature sets have been obtained from [15], while the Legendre quadrature sets have been obtained directly from [13].

Table 3-1 Tabuchi-Yamamoto Quadrature Sets

Polar Divisions	sin theta	omega (w)
1	0.798184	1.000000
2	0.363900	0.212854
	0.899900	0.787146
3	0.166648	0.046233
	0.537707	0.283619
	0.932954	0.670148

[[

]]

3.1.3. Adjusting Angles and Separation Distances to Align Tracks Along Boundaries

In two-dimensional problems, tracks reflect off the north and south boundaries of the problem, as well as off the east and west boundaries to the problem. This leads to unique azimuthal angles of motion between $0 \le \overline{\varphi} \le \pi/2$, and three reflected angles of motion between $\pi/2 \le \overline{\varphi} \le 2\pi$ – one reflected angle in each directional quadrant of the problem. In order to produce an exact solution to the characteristics equation, the end of each incident angle must align precisely with the beginning of its reflected counterpart along the problem boundary.

To ensure perfect reflection in two dimensions, track separations and streaming angles in the xy-plane of the problem are altered slightly based on the overall dimensions of the problem. If the system is of total width *X* and total height *Y*, then the total number of system widths spanned by a characteristic moving in the azimuthal direction of motion $\overline{\varphi}_i$, with a characteristic separation, d_i, is,

$$nx_i = \left| \frac{X \cos \overline{\varphi}_i}{d_i} \right| \tag{47}$$

and the total number of system heights spanned is,

$$ny_i = \left| \frac{Y \sin \overline{\varphi}_i}{d_i} \right| \tag{48}$$

In order to ensure that all tracks in direction $\overline{\varphi}_i$ align with their reflective counterparts along the boundary of the system, *nx* and *ny* are rounded up to the nearest integer values and the updated angle of streaming is re-calculated as,

$$\overline{\varphi}_i' = \tan^{-1}\left(\frac{ny_i' \cdot Y}{nx_i' \cdot X} \right), \text{ where } nx_i' = \text{int}\left(nx_i + 1\right) \text{ and } ny_i' = \text{int}\left(ny_i + 1\right) \tag{49}$$

along with the updated separation distance,

$$d_i' = \frac{X \cdot Y}{\sqrt{\left(ny_i' \cdot Y\right)^2 + \left(nx_i' \cdot X\right)^2}} \tag{50}$$

Using these angles and separations, the azimuthal set of parallel, equidistant tracks are traced across the system at angles between $0 \le \bar{\varphi}_i' \le \pi$. For angles of motion between $\pi \le \bar{\varphi}_i' \le 2\pi$, the previous tracks are used, allowing neutrons to travel in the opposite direction.

3.2. Ray Tracing

Cyclic trajectory ray tracing in LANCR02 is based on a method described in [10]. The ray tracing begins by laying a Cartesian coarse mesh over the problem geometry. The boundaries of each coarse mesh are determined by the pin array and various material zones of the problem, as illustrated by the bold outlines in Figure 3-2. Each coarse mesh defines a cell of a various type, where different cell types are distinguished by their contents. Cylinders are typically centered in a cell, although this is not a requirement and is often modified by the code to account for oversized water rods. Unique cell types have been created to handle pins along the edge of the channel shroud and in each corner of the channel, where the specific intricacies associated with the rounded box wall and the variation in wall thickness on the more modern bundle designs require special attention. Additional cell types have been created to handle the oversized water rods found in the various GE/GNF bundle designs and the water boxes, water diamonds, and water wings found in other popular bundle designs. Still more cell types exist to model the various portions of a control blade, and so on.

Once the Cartesian coarse mesh has been created and the various cells have been defined throughout the lattice, the ray tracing routine proceeds to subdivide each cell into smaller meshes that will define the flat flux regions of the problem. The default meshing for the vanish portion of a GE14 bundle design has been chosen for illustration in Figure 3-2. Mesh sub-divisions in cells that contain embedded cylinders are created at increments of either 22.5º or 45º angles, depending on the detail required for an accurate solution to the problem (larger pins require the finer azimuthal mesh). Note that the azimuthal mesh are used simply to define flat flux regions during the MoC solution and are not used to define azimuthal burnup zones per fuel pellet. An annular mesh is added to the coolant region of each pin cell, as illustrated in Figure 3-2, to help capture the steep thermal flux gradient in the coolant. Volumes are calculated for every mesh in the problem and are used to ratio track lengths at the end of the ray tracing process to ensure conservation during the MoC solution.

Once all mesh volumes have been calculated, the MoC routine is ready to begin ray tracing across the problem. Ray tracing takes place only for the azimuthal directions of motion between $0 \le \bar{\varphi}_i' \le \pi$ and only in the xy-plane of the problem. After the ray tracing has been completed, the tracks are raised out of the plane of the problem to each of the various polar angles and the lengths are adjusted accordingly.

A detailed description of ray tracing is included in Reference [10]. The ray tracing consists of determining the intersections of each characteristic with each mesh in the problem. The track lengths are calculated as the distance between successive intersections.

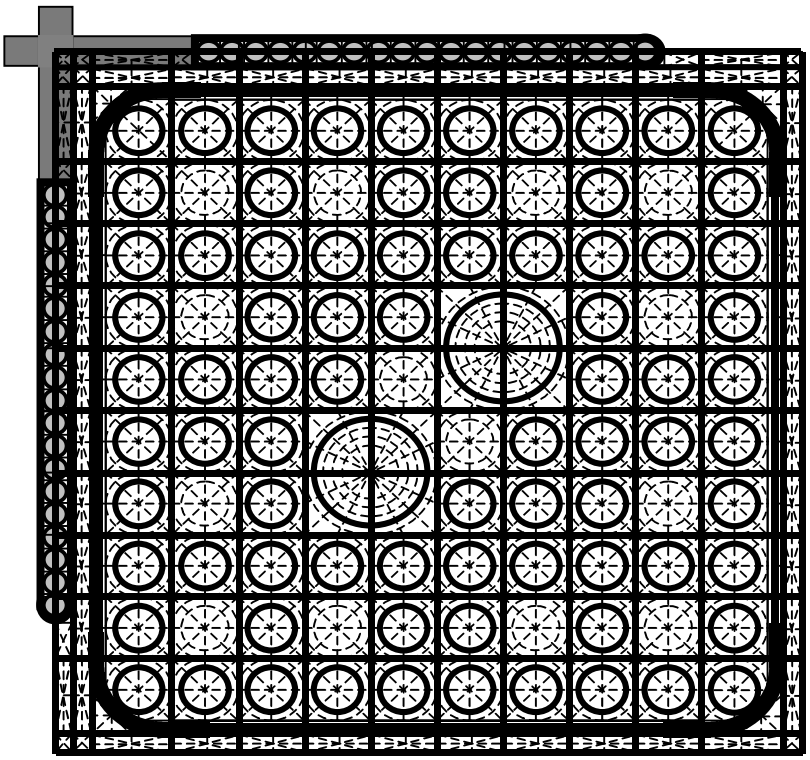

Figure 3-2 Example of MoC default fine-meshing for the vanish portion of a GE14 fuel design.

3.3. Preserving Mesh Volume

Once the ray tracing routine has calculated all track lengths in the xy-plane of the problem, the track lengths need to be modified to ensure that the solution to the characteristics equation preserves the volume of each mesh in the problem (see Figure 3-3 and Figure 3-4). For a given number of track segments crossing a mesh, the volume traced by the track segments moving in a specific direction is approximated as,

$$A_{i,n,approx} = \sum_k t_{k,n}(\bar{\varphi}_i') \cdot d_i' \tag{51}$$

where $t_{k,n}(\bar{\varphi}_i')$ is the length of the k'th track segment at azimuthal angle $\bar{\varphi}_i'$ in the xy-plane of the problem, crossing mesh n; and d_i' is the modified track separation at azimuthal angle $\bar{\varphi}_i'$, obtained from Eq. (49).

Each track segment is modified using the ratio between the true and the approximated volume of the mesh,

$$t'_{k,n}(\bar{\varphi}_i') = t_{k,n}(\bar{\varphi}_i') \cdot \frac{A_{n,true}}{A_{i,n,approx}} = t_{k,n}(\bar{\varphi}_i') \cdot \frac{A_{n,true}}{\sum_k t_{k,n}(\bar{\varphi}_i') \cdot d_i'} \tag{52}$$

The modified track lengths in the xy-plane from Eq. (52) are used in the solution to the characteristics equation.

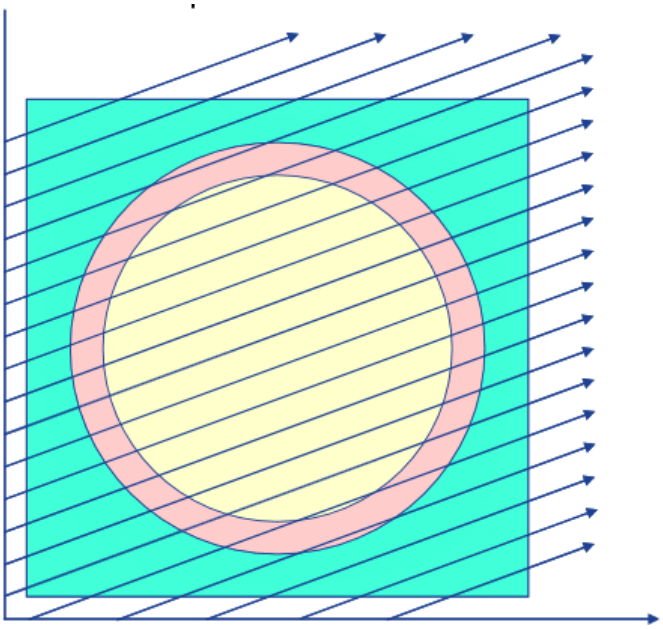

Figure 3-3 Example of tracks at equidistant intervals.

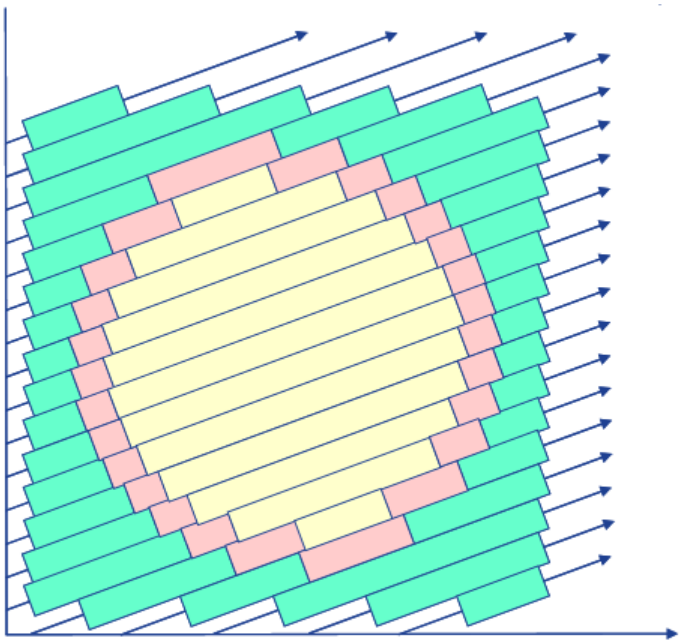

Figure 3-4 Example of adjusted tracks lengths to reproduce the true area of each mesh.

3.4. Solution to the Characteristics Equation

The equation of interest is Eq. (30), rewritten below in a simplified form,

$$\Phi_{k,n,out}^{G}(\bar{\varphi}_i,\bar{\theta}_j)=\hat{Q}_n^G+\exp\left[-\Sigma_{tr,n}^{G}\tau_{k,n}(\bar{\varphi}_i,\bar{\theta}_j)\right]\cdot\left(\Phi_{k,n,in}^{G}(\bar{\varphi}_i,\bar{\theta}_j)-\hat{Q}_n^G\right) \tag{53}$$

where $\tau_{k,n}(\bar{\varphi}_i',\bar{\theta}_j)=t_{k,n}'(\bar{\varphi}')/\sin\bar{\theta}_j$ is the modified track length after being lifted out of the xy-plane of the problem to the appropriate polar angle; and $\hat{Q}_n^G=q_n^G/4\pi\Sigma_{tr,n}^G$ is the term containing the angular source. [[

]] The scalar source term included in Eq. (53) is calculated as,

$$q_n^G=\sum_{G'}\left(\Sigma_{s,n}^{G'\to G}+\frac{\Sigma_{p,n}^{G'\to G}}{k^{\infty}}\right)\phi_n^{G'} \tag{54}$$

where the production cross section is defined as $\Sigma_{p,n}^{G'\to G}=\chi_n^G\sum_{G'}\nu\Sigma_{f,n}^{G'}$.

The scalar flux in Eq. (54) – for any given mesh – is obtained from Eq. (31),

$$\phi_n^G=\sum_j\sum_i\sum_k\bar{\Phi}_{k,n}^{G}(\bar{\varphi}_i',\bar{\theta}_j)\cdot\omega_i\cdot\omega_j \tag{55}$$

After substituting the expression for the average angular flux across a mesh into Eq. (55), the following expression for the scalar flux results, where all sources are considered isotropic (using transport-corrected cross sections to account for anisotropic effects),

$$\phi_n^G=\hat{Q}_n^G+\frac{1}{\Sigma_{tr,n}^G}\sum_j\sum_i\sum_k\frac{\Delta_{k,n}^{G}(\bar{\varphi}_i,\bar{\theta}_j)\cdot\omega_i\cdot\omega_j\cdot\sin\bar{\theta}_j}{t_{k,n}'(\bar{\varphi}_i)} \tag{56}$$

where $\Delta_{k,n}^{G}(\bar{\varphi}_i',\bar{\theta}_j)=\Phi_{k,n,in}^{G}(\bar{\varphi}_i',\bar{\theta}_j)-\Phi_{k,n,out}^{G}(\bar{\varphi}_i',\bar{\theta}_j)$; and $\tau_{k,n}(\bar{\varphi}_i',\bar{\theta}_j)$ has been replaced with $t_{k,n}'(\bar{\varphi}_i')/\sin\bar{\theta}_j$. Substituting Eq. (54) into Eq. (56) the scalar flux is

$$\phi_n^G=\hat{Q}_n^G+\frac{1}{\Sigma_{tr,n}^G A_{true}}\sum_j\sum_i\omega_{ij}\sum_k\Delta_{k,n}^{G}(\bar{\varphi}_i,\bar{\theta}_j) \tag{57}$$

where $\omega_{ij}=\omega_i\cdot d_i'\cdot\omega_j\cdot\sin\bar{\theta}_j$.

Equations (53), (54), and (57) constitute the set of equations that need to be solved in order to obtain a solution to the transport equation.

3.5. Acceleration

3.5.1. Spatial Acceleration

The scalar flux is accelerated spatially using a simple coarse mesh rebalance (CMR) throughout the system [13],[16]. Coarse meshes are defined at the beginning of the ray tracing routine, as illustrated by bold outlines in Figure 3-2. The balance equation to be solved in each coarse mesh is,

$$\left[\sum_{n\in N}\Sigma_{r,n}^{G}\phi_{n}^{G}V_{n}+\sum_{s\in N}\psi_{s,N,out}^{G}A_{s,N}\right]\cdot f_{N}^{G}=\sum_{n\in N}q_{n}^{G}V_{n}+\sum_{s\in N}\psi_{s,N,in}^{G}A_{s,N}\cdot f_{N'}^{G} \tag{58}$$

where n represents the fine-mesh subdivisions and material regions that make up a coarse mesh, N; s represents the surfaces to the coarse mesh; $\psi_{s,N,out}^{G}$ represents the outward-directed scalar flux along surface s of coarse mesh N; $A_{s,N}$ represents the surface area; and N' represents the coarse mesh that shares surface s with coarse mesh N.

The integrated surface flux, $\psi_{s,N,out}^{G}A_{s,N}$, is accumulated as Eq. (53) is solved. The contribution to the outward-directed integrated angular flux along a coarse mesh surface is calculated as,

$$\psi_{s,N,out}^{G}A_{s,N}=\sum_{j}\sum_{i}\omega_{ij}\sum_{k}\Phi_{k,n,out}^{G}(\bar{\varphi}_{i}',\bar{\theta}_{j}) \tag{59}$$

where the summation is only accumulated if $\Phi_{k,n,out}^{G}(\bar{\varphi}_{i}',\bar{\theta}_{j})$ is along the edge of coarse mesh N. This information is obtained from the ray tracing routine.

Eq. (58) is solved iteratively for the balance factors, f_{n}^{g} , using a red-black iteration scheme. Once the balance factors have been determined, the scalar flux is updated,

$$\phi_{n}^{G}=\phi_{n}^{G}\cdot f_{N}^{G} \tag{60}$$

for all mesh subdivisions, n, within coarse mesh region N. The CMR calculation is performed at the end of each inner iteration.

Since the CMR acceleration scheme can be unstable under certain conditions, the acceleration is applied as long as the total number of outer iterations is below a reasonable level. If the number of outer iterations exceeds this level, the CMR is disengaged and the flux is solved without any spatial acceleration. Such conditions rarely, if ever, exist for typical single-lattice problems common to LWR reactor analysis.

Implementation of the CMR acceleration scheme can usually reduce the total number of outer iterations by a factor of 3 to 4, depending on the type of problem being analyzed. It should be mentioned that there usually exists an excellent flux guess from a previous state point from which to start each calculation. Because of this, no more than a dozen outer

iterations are often needed to fully converge the flux, so the acceleration scheme is of minimal importance.

3.5.2. Energy Acceleration

Following completion of an outer iteration, a fundamental mode rebalancing of the group flux distribution is performed in order to properly normalize the flux and ensure neutron conservation. The fundamental mode calculation is performed on an equivalent homogeneous system using flux- and volume-weighted cross sections from the heterogeneous calculation, as in Eq. (38). The fundamental mode equation to be solved is,

$$\overline{\phi}_{FM}^{G} = \overline{q}^{G} / \overline{\Sigma}_{r}^{G} \tag{61}$$

where the source term does not include self scattering and the removal cross section is defined as in Eq. (37). The source term is calculated as $\overline{q}^{G} = \sum_{G' \neq G} \overline{\Sigma}_{s}^{G' \to G} \overline{\phi}_{FM}^{G'} + \overline{\chi}^{G}$ and the corresponding eigenvalue to the system is calculated as $k^{\infty} = \sum_{G'} \nu \overline{\Sigma}_{f}^{G'} \overline{\phi}_{FM}^{G'}$, where the flux has been normalized such that there is one neutron being absorbed in the system.

Due to upscattering in the thermal energy groups, the solution to Eq. (61) defines an iterative process and the fundamental mode equation is solved directly, with no acceleration. Following the solution to Eq. (61), the scalar flux distribution from Eq. (60) is scaled using the rebalance factors,

$$\hat{\phi}_{n}^{G} = \phi_{n}^{G} \cdot \frac{\overline{\phi}_{FM}^{G}}{\sum_{n} \phi_{n}^{G} V_{n}} \tag{62}$$

where the summation in the denominator of Eq. (62) is over all mesh in the problem.

The fundamental mode rebalance calculation can reduce the number of outer iterations needed to converge the flux by about a factor of 2.

3.6. Convergence

This section describes the convergence criteria used in the LANCR02 solution scheme.

3.6.1. Convergence of the Angular Flux

For each energy group, *G*, there is an initial value for the inward-directed angular flux along the surface of the problem, in azimuthal direction $\overline{\varphi}_{i}'$, polar direction $\overline{\theta}_{j}$, along track *k*, which is denoted by $\Phi_{k,in}^{G}(\overline{\varphi}_{i}', \overline{\theta}_{j})$. The track is followed until another boundary to the system is reached, at which point the angular flux, $\Phi_{k,out}^{G}(\overline{\varphi}_{i}', \overline{\theta}_{j})$, is directed outward. This becomes the value for the inward-directed angular flux in the reflected (or periodic) direction, $\Phi_{k',in}^{G}(\overline{\varphi}_{i'}', \overline{\theta}_{j}) = \Phi_{k,out}^{G}(\overline{\varphi}_{i}', \overline{\theta}_{j})$. The new value replaces the previous value for the inward-

directed angular flux in the reflected direction $(\overline{\varphi}'_i, \overline{\theta}'_j)$. The difference between the two values – the value of the inward-directed boundary angular flux at the end of the previous iteration, and the value at the end of the present iteration – will approach zero as the solution converges. When all inward-directed boundary angular flux values have changed by less than a certain criterion, ε, from their values at the end of the previous iteration, the angular flux for that particular energy group is assumed to be converged,

$$\left| \frac{\Phi^G_{k,in}(\overline{\varphi}'_i, \overline{\theta}_j)\Big|_{new} - \Phi^G_{k,in}(\overline{\varphi}'_i, \overline{\theta}_j)\Big|_{old}}{\Phi^G_{k,in}(\overline{\varphi}'_i, \overline{\theta}_j)\Big|_{old}} \right| < \varepsilon \tag{63}$$

Eq. (63) must hold true for all *i*'s, *j*'s, and *k*'s in all energy groups in order to satisfy a fully converged solution to the problem.

3.6.2. Convergence of the Scalar Flux

At the end of each inner iteration, in addition to testing for convergence of the inward-directed boundary angular flux, the scalar flux is also tested for convergence. The same principle applies here as for the angular flux. The iteration begins with some value for the scalar flux in group *G*, $\phi^G_n\Big|_{old}$. This value is used to calculate the source term before solving for the new flux distribution. With the source distribution frozen in group *G*, a new scalar flux distribution, $\phi^G_n\Big|_{new}$, is calculated. The difference between the old and new value of the scalar flux will approach zero as the solution converges. As in the case of the angular flux, convergence is declared when the following statement is satisfied in every mesh, every energy group,

$$\left| \frac{\phi^G_n\Big|_{new} - \phi^G_n\Big|_{old}}{\phi^G_n\Big|_{old}} \right| < \varepsilon \tag{64}$$

3.6.3. Convergence of the Eigenvalue

Before starting an outer iteration, the eigenvalue for the old flux distribution is calculated, k^∞. As the fission source distribution converges, so too will the eigenvalue. The convergence of the eigenvalue is checked from one iteration to the next,

$$\left| \frac{k^\infty\Big|_{new} - k^\infty\Big|_{old}}{k^\infty\Big|_{old}} \right| < \varepsilon \tag{65}$$

Eq. (65) will always be satisfied if both Eqs. (63) and (64) are satisfied. That is, the eigenvalue will always be converged if the flux distribution is converged. For this reason, satisfying Eq. (65) is relatively irrelevant.

4. POWER DISTRIBUTION CALCULATION

4.1. Overview

The power generated in a fuel rod is the sum of energy from gamma and beta decay, as well as kinetic energy from fission. The various contributions to the power are calculated as;

4.1.1. Kinetic energy of fission fragments and neutrons in fuel rod *I*

$$E_{kinetic,I} = \sum_{iso} q'_{fission,iso} \sum_{i \in I} \sum_{G} N_{iso,i} \sigma^{G}_{f,iso,i} \phi^{G}_{i} V_{i} \tag{66}$$

where

$q'_{fission,iso}$ = kinetic energy of fission fragments and neutrons from fission of nuclide *iso*
$N_{iso,i}$ = Number density of nuclide *iso* in mesh *i*
$\sigma^{G}_{f,iso,i}$ = fission cross section of nuclide *iso* in mesh *i*, group *G*
ϕ^{G}_{i} = neutron flux in mesh *i,* group *G*
V_{i} = volume of mesh *i*

4.1.2. Total gamma energy deposited in fuel rod *I*

$$E_{\gamma,I} = \sum_{i \in I} \sum_{\gamma} \Sigma^{\gamma}_{e,i} \phi^{\gamma}_{i} V_{i} \tag{67}$$

where

$\Sigma^{\gamma}_{e,i}$ = gamma energy deposition cross section from the gamma cross section library
ϕ^{γ}_{i} = gamma flux in mesh *i,* gamma group γ

4.1.3. Beta energy due to absorption in fuel rod *I*

$$E_{\beta,I} = \sum_{iso} q'_{\beta,iso} \sum_{i \in I} \sum_{G} N_{iso,i} \sigma^{G}_{a,iso,i} \phi^{G}_{i} V_{i} \tag{68}$$

where

$q'_{\beta,iso}$ = beta energy released per absorption in nuclide *iso* from the ENDF/B decay libraries
$\sigma^{G}_{a,iso,i}$ = neutron absorption cross section of nuclide iso in mesh *i*, group *G*

4.1.4. Loss of kinetic energy due to fast neutron capture in fuel rod I

$$E_{c,I} = \sum_{iso} \sum_{i \in I} \sum_{G > 5.53 keV} q'^{G}_{c,iso} N_{iso,i} \sigma^{G}_{c,iso,i} \phi^{G}_{i} V_{i} \tag{69}$$

where

$q'^{G}_{c,iso}$ = loss of neutron kinetic energy due to neutron capture in group *G*

$\sigma^{G}_{c,iso,i}$ = neutron capture cross section of nuclide iso in mesh *i*, group *G*

[[

]]

5. DEPLETION MODEL

5.1. Various Types of Depletion Calculations

Three types of depletion calculations are provided in LANCR02: (1) a fuel depletion calculation; (2) a control blade depletion calculation – with or without fuel depletion; and (3) a shutdown cooling calculation.

5.1.1. Fuel Depletion

The fuel depletion calculation is used for typical fuel/core design calculations. Any pellet can be sub-divided into multiple material zones of equal volume. Each material zone is modeled using a unique set of number densities. [[

]]

5.1.2. Control Blade Depletion

The control blade depletion calculation is used to deplete the absorber materials in a control blade. The control blade materials can be depleted while the fuel isotopes are held constant, or the control blade and fuel can be depleted at the same time. Absorber rods may be sub-divided annularly into individual material regions or modeled whole. Each absorber rod in a control blade wing may be its own unique depletion region or any number of rods may be grouped together and depleted as an average.

5.1.3. Cooling Calculation

The cooling calculation is engaged if the cooling option is selected and time after shutdown is greater than 0.0. Through the cooling calculation, short-lived nuclides are depleted before entering the neutron transport calculation. Alternatively, the user may use no Xenon option, which sets all I-135 and Xe-135 number densities to zero, simulating a shut down period of a few days. This option does not simulate the build-up of Sm-149 following shut down.

5.2. Depletion Calculation

5.2.1. Equations to be Solved

The depletion chains contained in LANCR02 are diagrammed in Figure 5-1 through Figure 5-5. The depletion equation to be solved is a first-order differential equation of the type,

$$\frac{dN_{iso}}{dt} = \sum_{iso'} u_{iso,iso'}\lambda_{iso'}N_{iso'} + \sum_{iso'} v_{iso,iso'}(\sum_g \sigma^g_{c,iso'}\phi''^g)N_{iso'} + \sum_{iso'} w_{iso,iso'}(\sum_g \sigma^g_{(n,2n),iso'}\phi''^g)N_{iso'} + \sum_{iso'} \gamma_{iso,iso'}(\sum_g \sigma^g_{f,iso'}\phi''^g)N_{iso'} - \left\{\lambda_{iso} + (\sum_g \sigma^g_{a,iso}\phi''^g) + (\sum_g \sigma^g_{(n,2n),iso}\phi''^g)\right\}\cdot N_{iso} \quad (70)$$

where $u_{iso,iso'}$, $v_{iso,iso'}$, $w_{iso,iso'}$ are branching ratios for decay, neutron capture, and (n,2n) reactions, respectively; λ_{iso} is the decay constant for isotope *iso*; $\gamma_{iso,iso'}$ is the fission yield; and ϕ''^g is the flux distribution from the leakage-corrected flux from the MoC solution. Eq. (70) has a solution of the form,

$$N_{iso}(\Delta t) - N_{iso}(0) = (Q - \tilde{\lambda}_{iso}N_{iso}(0))\ \frac{(1-e^{-\tilde{\lambda}_{iso}\cdot\Delta t})}{\tilde{\lambda}_{iso}} \quad (71)$$

where the effective decay constant, $\tilde{\lambda}_{iso}$, is equal to $\tilde{\lambda}_{iso} = \lambda_{iso} + (\sum_g \sigma^g_{a,iso}\phi''^g) + (\sum_g \sigma^g_{n2n,iso}\phi''^g)$ and the production term, Q, is assumed constant over a small time interval, Δt.

The solution to Eq. (70) is obtained using a 4th order Runge-Kutta-Gill algorithm for the predictor step. For the corrector step, the effective decay constant is assumed to vary linearly over the time step, Δt, and

$$\frac{dN_{iso}}{dt} = -(\lambda_0 + \lambda_1 t)N_{iso} + \bar{Q} \quad (72)$$

where λ_0, λ_1, and $\bar{Q}$ are obtained from the solution during the predictor step. The corrector step solves for the analytic solution explicitly,

$$N(t) = N(0)e^{-\bar{\lambda}\cdot t} + 2a\cdot\frac{\bar{Q}}{\lambda_0}\cdot\left[F(b) - e^{-\bar{\lambda}\cdot t}F(a)\right]$$

$$a = \frac{\lambda_0}{\sqrt{2\lambda_1}} \quad b = \frac{\lambda_0 + \lambda_1 t}{\sqrt{2\lambda_1}} \quad (73)$$

where $\bar{\lambda}$ is the average decay constant from the predictor solution; and *F(x)* is a Dawson's integral,

$$F(x) = e^{-x^2}\int_0^x e^{u^2}du \quad (74)$$

Solution to Eq. (73) supplies the final number densities at the end of the time step.

5.3. Dual Time Step Model

For fuel mixtures that contain UO_2 or MOX isotopes, depletion step sizes as large as 2 GWd/ST (GWd/ST = Gigawatt day per short ton) are sufficient to accurately deplete the heavy metal and build in the higher actinides and fission products. For fuel mixtures that contain gadolinium, however, a time step size of 2 GWd/ST can introduce large errors into the results from the lattice physics code. This sensitivity is caused by the large spatial self-shielding of the Gd-155 and Gd-157 isotopes that create rapid changes in the thermal flux distribution across the fuel pellet as the gadolinium depletes. To accurately capture the depletion rate of the gadolinium, time step sizes on the order of 0.2 GWd/ST are typically required at the lattice level.

To account for the different depletion rates of the various isotopes, dual time steps in LANCR02 are used to handle lattice designs that contain fuel pins with gadolinium. The complete series of 1-D pin cell calculations, followed by the 2-D RM calculation and 2-D MoC calculation, are performed at lattice depletion time step increments of 1 GWd/ST. In between complete lattice calculations, gadolinium pins are depleted at 0.2 GWd/ST time step increments by re-performing only the 1-D pin cell calculations and using the flux distribution from the previous RM and MoC calculations to augment the updated pin cell flux.

The depletion scheme is expressed with Eqs. (27), (37), (38) and the updated pin cell flux, ψ_i^g,

$$\tilde{\psi}_i^g = \psi_i^g \cdot \frac{\phi_I^g V_I}{\sum_{i \in I} \psi_i^g V_i} \tag{75}$$

$$\psi_i'^g = \tilde{\psi}_i^g \cdot \frac{\phi_i^G}{\sum_{g \in G} \tilde{\phi}_i^g} \tag{76}$$

$$\psi_i''^g = \psi_i'^g \cdot \frac{\Psi^g \cdot \sum_i V_i}{\sum_{i \in I} \psi_i'^g V_i} \tag{77}$$

where ϕ_I^g is the fine-group flux from the most recent RM calculation; $\tilde{\phi}_i^g$ is the most recent fine-group condensation flux; ϕ_i^G is the transport-group flux from the most recent MoC calculation; and Ψ^g is the fine-group critical flux from the most recent fundamental mode calculation.

The dual time steps continue until the Gd-155 and Gd-157 isotopes have been sufficiently depleted from all pins, at which time the code reverts to standard default time steps of 2 GWd/ST.

5.4. Control Blade Depletion

A control blade can be inserted into the NW corner of the lattice for any calculation that contains an outer water gap. By default, the absorber isotopes in the control blade are not depleted, even if the problem being analyzed is a depletion case. However, if requested, the absorber isotopes in the control blade can also be depleted. The absorber isotopes in the control blade can be depleted together with the burnable isotopes in the fuel pellets, or the absorber isotopes in the control blade can be depleted without depleting the burnable isotopes in the fuel pellets.

5.4.1. Creating Depletion Zones

Any number of depletion zones may be created in the control blade. Depletion zones are specified externally. A depletion zone is assigned to each absorber rod in the control blade along with the number of absorber rods in the control blade.

Isotopics are averaged for each absorber zone. [[

]]

5.4.2. Annular Depletion Rings

[[

]]

5.5. Choice of Time Step

LANCR02 provides for three types of time steps: MWd/MT, MWd/ST, and day. When the day option is specified, time intervals are calculated using the relation,

$$\Delta t = \frac{\Delta E \cdot FNA}{const \cdot P_0} \tag{78}$$

where Δt is the time interval in days; ΔE is the exposure step size in either MWd/MT or MWd/ST; P_0 is the power density in W/cm^3; $const$ is a constant equal to either 0.602472 for MWd/MT or 0.546576 for MWd/ST; and FNA is the initial density of heavy metal in g/cm^3.

5.6. Fissile and Fertile Chain

The fissile and fertile chain is diagram is shown in Figure 5-1.

5.7. Fission Product Chain

The fission product (FP) chain contains two pseudo FPs (PFP1 and PFP2) that are used as collection bins at the end of several sub-chains. The pseudo FPs have no cross sections associated with their number densities. The FP chain diagrams are illustrated in Figure 5-2 through Figure 5-4.

5.8. Burnable Absorber Chain for Control Blade Isotopes

Two elements used as absorber material in control blades can be modeled as time-dependent in LANCR02. The B-10 and Hf depletion chains are represented in Figure 5-5.

[[

]]

Figure 5-1 Fissile and fertile chain diagram

[[

]]

Figure 5-2 FP chain diagram (1 of 3)

[[

]]

Figure 5-3 FP chain diagram (2 of 3)

[[

]]

Figure 5-4 FP chain diagram (3 of 3)

[[

]]

Figure 5-5 Boron and Hafnium chain diagram

6. VOID DISTRIBUTION MODEL

6.1. Overview

LANCR02 is capable of superimposing a non-uniform void distribution across the in-channel flow area of the lattice based on local pin powers. The impact of this option is most visible over the range of void fraction levels from 0.25 to 0.55. Obviously, at void fractions of 0.0 and 1.0, there is nothing to be distributed.

The non-uniform void model re-distributes the void to the high energy regions of the lattice. Consequently, the non-uniform void option will result in an increase in control rod worth, a more rapid depletion rate of the gadolinium isotopes, and a reduction in pin peaking factors.

The void distribution model can be turned on and off through user input.

6.2. Power Distribution Calculation

In order to implement the distributed void model non-uniform void model, a pin-wise power distribution is required. [[

]]

6.3. Void Distribution Model

[[

(79)

(80)

(81)

(82)

Table 6-1

Table 6-2

Table 6-3

]]

7. BUNDLE GEOMETRIES

7.1. Modeling Various Lattice and Assembly Geometries

LANCR02 can model various geometry configurations including: single pin cells, square arrays of NxN fuel-rods with or without vanished rods, non-fuel pins, and various internal water rod configurations. The array of fuel pin can be optionally surrounded by gaps of varying sizes, and include several channel box and control blade geometries. Typical configurations are listed in Table 7-1 and illustrated in Figure 7-1 through Figure 7-5.

All configurations listed, except the water diamond, are treated explicitly with no significant geometry approximations. The water diamond is approximated by modeling a water box.

The Method of Characteristics transport solution is flexible and extensible to any two-dimensional geometry configuration.

The Method of Characteristics transport solution is flexible and extensible to any two-dimensional geometry configuration. The only practical limitation to the geometry is the internal automation used to trace rays over current LWR designs. However, these ray tracing routines can easily be extended to model any future lattice or blade designs without changing the underlying methodology. There are other parts of the LANCR02 methodology (namely the pin cell model) that limit LANCR02 to circular fuel pins.

Table 7-1 Standard Geometry Configurations Treated

Lattice		Remarks
Single fuel rod cell		Figure 7-1
Square array of fuel rods		Figure 7-2
GNF/GE fuel assembly	8x8	Figure 7-3
	9x9	
	10x10	
Water Box	9x9	With central water box
	9x9	With offset water box
	10x10	Figure 7-4
Water Diamond and Water Cross	8x8	No central water diamond
	10x10	No central water diamond
	10x10	Figure 7-5

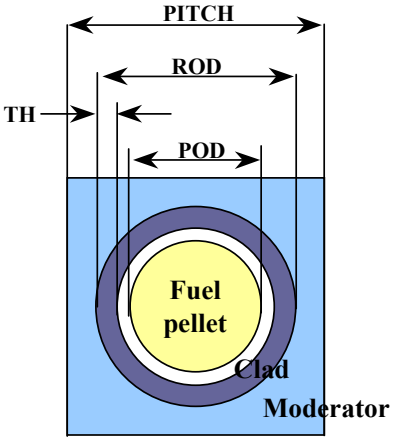

Figure 7-1 Single pin cell

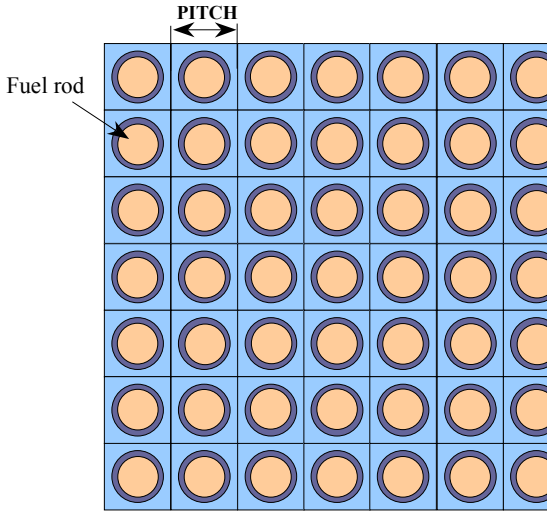

Figure 7-2 Square array of rods.

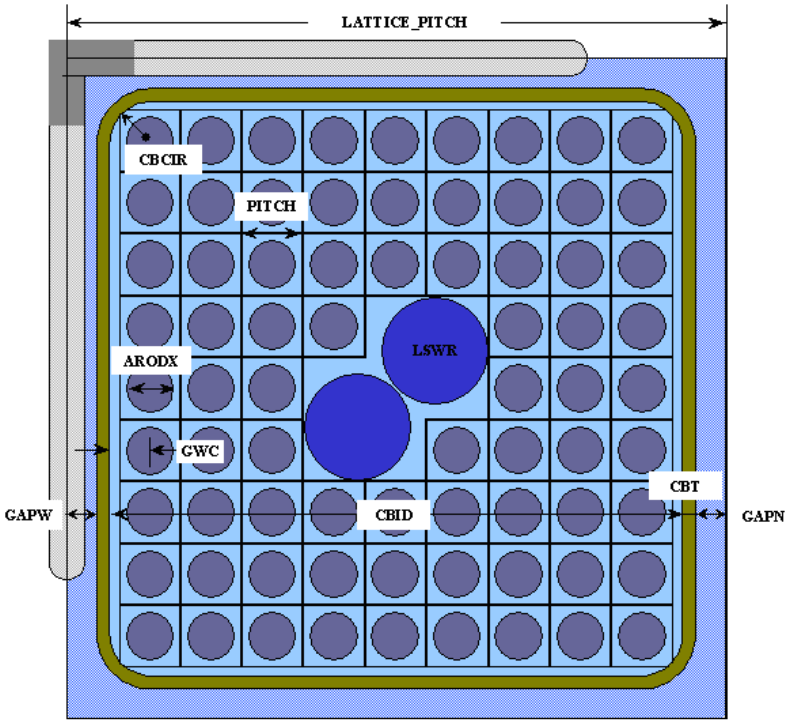

Figure 7-3 GE 9x9 bundle design.

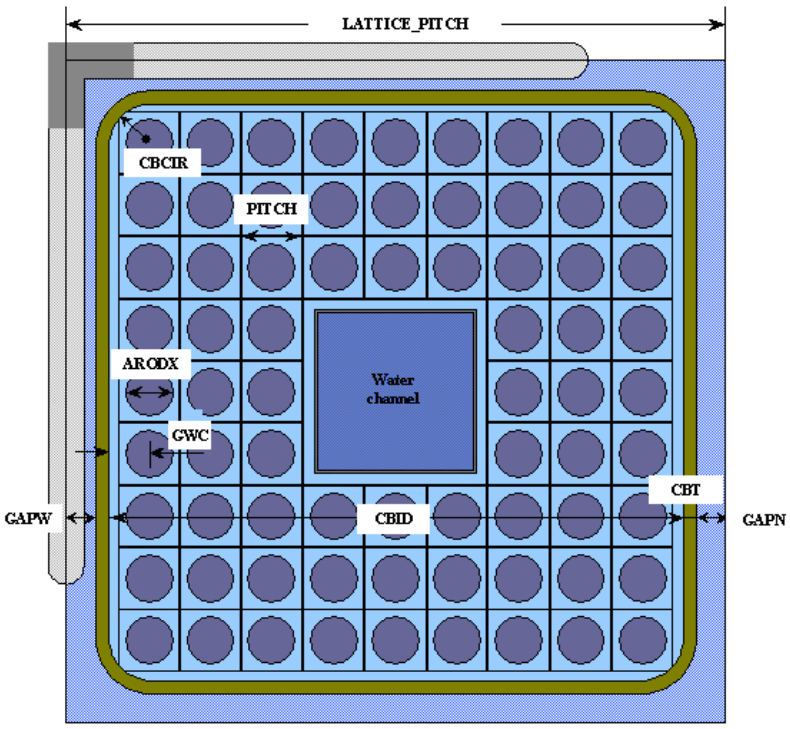

Figure 7-4 Water Box 9x9 bundle design with central water box.

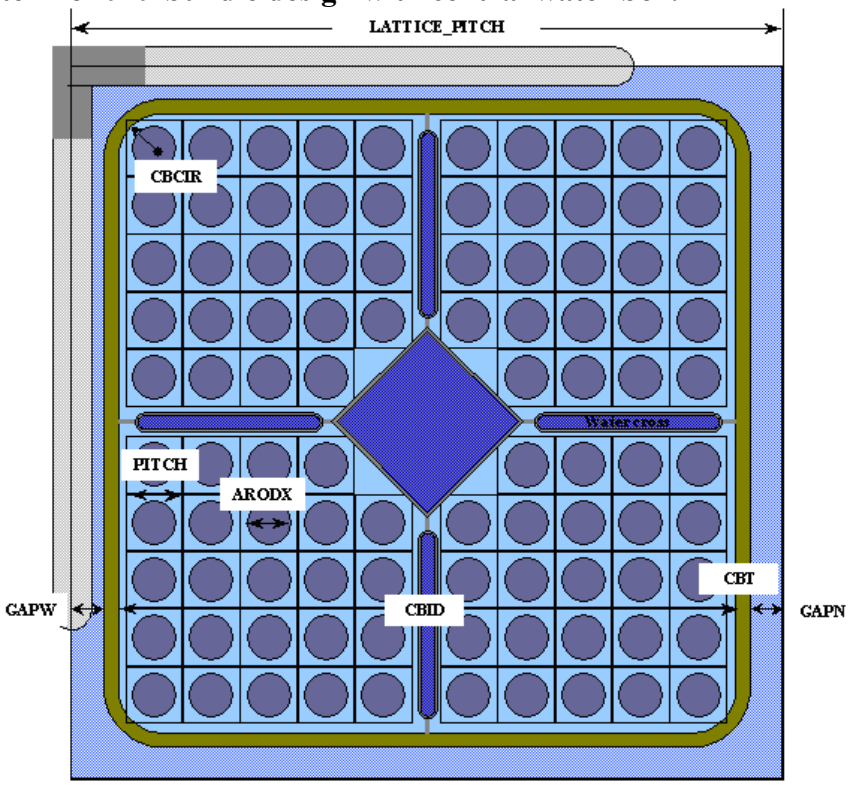

Figure 7-5 Water Cross bundle design with central water diamond.

7.2. Modeling Various Channel Geometries

Channels of uniform thickness are modeled precisely by the code, including the rounded box corners. Channels of non-uniform thickness – so-called thick-thin channels – are modeled precisely if the channel does not contain a side notch. For channels that contain side notches, the thin width of the channel is modified to preserve the total volume of the channel material.

7.3. Modeling Various Control Blade Geometries

LANCR02 treats several types of control blades, as listed in Table 7-2.

Table 7-2 Standard Control Blade Geometries Treated.

Type	Calculation model
Conventional B_4C Blade	Pin type model
Hitachi Hf Rod Control Blade	
B_4C-Hf Hybrid Control Blade	
Marathon Control Blade	
ABB Control Blade	
Grey-nose Control Blade	Plate type models
Toshiba Hf Plate Control Blade	
ABWR Hf Flat Tube Control Blade	

The composition of the absorber material is specified via input, which allows the user control over the fraction of B-10 in the B_4C mixture.

7.4. Modeling Various Rod Geometries

LANCR02 models fuel rods and non-fuel cells explicitly.

7.4.1. Fuel Rod Cell

There are 3 different types of fuel rods that can be modeled: (1) UO_2 fuel rod; (2) MOX fuel rod; and (3) UO_2 fuel rod containing burnable absorber. [[

]]

7.4.2. Non-Fuel Cell

There are seven separate non-fuel cells that can be modeled: (1) vanish cell containing only coolant; (2) plenum rod containing spring material ; (3) water rod occupying a single pin cell location; (4) oversized water rod occupying 4 pin cell locations; (5) oversized water rod occupying 3.5 pin cell locations (i.e., two rods occupying 7 pin cell locations); (6) oversized

water box occupying 9 pin cell locations; and (7) oversized water diamond occupying 4 pin cell locations.

7.5. Modeling the BWR Instrument Assembly Geometry

[[

]]

The instrument assembly model is illustrated in Figure 7-7. In LANCR02, the instrument assembly consists of only 3 regions: (1) the outer cover tube; (2) the insulation region of the tube; and (3) the central anode/cathode region of the sensor.

[[

]]

[[

]]

Figure 7-6 Phantom Instrument Assembly Model.

[[

]]

Figure 7-7 Explicit Instrument Assembly Model.

8. OUTPUT

LANCR02 produces output to five separate files. There are three ASCII output files that summarize results such as eigenvalue, pin-wise fission and power distributions, and lattice-averaged isotopic inventories. The ASCII files include: (1) an output file; (2) a summary file; and (3) an error file that is written only if the code aborts execution. There are two binary data files that may be written. One file is a wrap-up file that contains all data necessary to perform a branch calculation, and the other file contains data that is to be transferred to the core simulator.

8.1. ASCII Output Edit

The following quantities are edited to the ASCII output file.

- Time : core operation period (days)
- Exposure : lattice-averaged exposure (MWd/t)
- Assembly average few group macroscopic cross sections
- Few group dependent assembly discontinuity factors
- Few group dependent assembly-corner discontinuity factors
- Lattice-averaged isotope-wise neutron balance tables
- Rod-by-rod relative fission distribution and its peaking factor
- Rod-by-rod relative power distribution and its peaking factor
- Rod-by-rod relative exposure distribution and its peaking factor
- Rod-by-rod gamma energy deposition distribution
- Kinetics parameters including effective delayed neutron fraction, prompt neutron life time.
- Effective MeV/fission
- Average fission yields and microscopic capture cross sections for several important FPs, and so on.
- Summary table of k-infinity's and local peaking factors

8.2. Nomenclature

g	= few-group energy structure
m_{iso}	= material number from cross section library (e.g. $m_{Pu\text{-}241}$=26)
r	= material region (e.g., fuel, clad, coolant, etc.)
s	= surface of the assembly
h	= 6-group delayed neutron structure
i	= fine-group energy structure
j	= gamma source group structure
E	= exposure
$dr = V(r)$	= volume of material region r
V_{ass}	= volume of fuel assembly
V_{clad}	= total volume of all clad
V_{fuel}	= total volume of all fuel pellets

m_{iso} =order of nuclide *iso* in the nuclide library

$N_{iso}(r)$ = atomic number density for nuclide *iso*; at position *r*

A_{iso} = atomic mass of nuclide *iso*

ρ_{iso} = density for nuclide *iso*, in (g/cc)

$\sigma_{x,iso}(g,r)$ = microscopic cross section for reaction type x; of nuclide *iso*; in energy group *g*; at position *r*.

$\phi(g,r)$ = neutron flux in energy group g; at position r

$\psi(g,s)$ = neutron surface flux in energy group *g*; at surface position *s*

$\chi_{iso}(i,h)$ = delayed neutron fission spectrum of nuclide *iso*; for neutrons born in energy group *i*; to be deposited in delayed group *h*

$\Psi(i)$ = neutron flux in group *i* from fundamental mode calculation

$\Psi^{\dagger}(i)$ = adjoint flux in group *i* from fundamental mode calculation

NN = Narrow-Narrow gap

NW = Narrow-Wide gap

WW = Wide-Wide gap

WN = Wide-Narrow gap.

8.3. Binary Output

The following data are stored in the binary output file.

ACPU40: macroscopic capture cross section for Pu-240

$$ACPU40(g) = \frac{\int_{ass} N_{Pu-240}(r)\sigma_{c,Pu-240}(g,r)\phi(g,r)dr}{\int_{ass} \phi(g,r)dr}$$

ADBI: lattice-averaged atomic number densities of each nuclide

$$ADBI(m_{iso}) = \frac{1}{V_{ass}} \int_{ass} N_{iso}(r)dr$$

ADBI41: lattice-averaged atomic number density of Pu-241

$$ADBI41 = ADBI(m_{Pu-241} = 26)$$

ADI : fuel-averaged atomic number density of heavy isotope iso

$$ADI(m_{iso}) = \frac{1}{V_{fuel}} \int_{fuel} N_{iso}(r)dr$$

ADP39 : fuel-averaged atomic number density of Pu-239

$$ADP39 = ADI(m_{Pu-239} = 24)$$

ADP40 : fuel-averaged atomic number density of Pu-240

$$ADP40 = ADI(m_{Pu-240} = 25)$$

ADP41 : fuel-averaged atomic number density of Pu-241

$$ADP41 = ADI(m_{Pu-241} = 26)$$

ADU : fuel-averaged atomic number density of all heavy isotopes

$$ADU = \sum_{iso=heavy\ isotopes} ADI(m_{iso})$$

ALAMDA : decay constant of delayed neutrons in delayed group h

$$ALAMDA(h) = \frac{\sum_{iso=fissiles} \lambda_{iso}(h) \cdot \beta_{iso}(h) \cdot \sum_{g} N_{iso} \nu\sigma_{f,iso}(g)\phi(g)}{\overline{\beta}(h) \cdot \sum_{g} \nu\overline{\Sigma}_{f}(g)\phi(g)}$$

where $\beta_{iso}(h)$ is the delayed neutron fraction for nuclide *iso*, in delayed group *h*; and $\lambda_{iso}(h)$ is its decay constant. The averaged delayed neutron fraction, $\overline{\beta}(h)$, is calculated as,

$$\overline{\beta}(h) = \frac{\sum_{iso=fissiles} \beta_{iso}(h) \cdot \sum_{g} N_{sio} \nu\sigma_{f,iso}(g)\phi(g)}{\sum_{g} \nu\overline{\Sigma}_{f}(g)\phi(g)}$$

AVLATF : few-group lattice-averaged flux

$$AVLATF(g) = \frac{1}{V_{ass}} \int_{V_{ass}} \phi(g,r)dr$$

BDC : few-group boundary diffusion coefficient for each assembly surface

$$BDC(g) = \frac{\int_{S_{ass}} D(g,r)\psi(g,r)dS}{\int_{S_{ass}} \psi(g,r)dS}$$

where $\psi(g,r)$ is the surface flux at position *r* and the integral is performed over one assembly surface only. There are 4 BDC values in the binary file: (1) north; (2) east; (3) south; (4) west.

BETAC : alternate effective delayed neutron fraction for delayed group h

The effective delayed neutron fraction accounts for the fact that delayed neutrons are born at energies lower than those of prompt neutrons and, hence, do not contribute to fast fission and have smaller leakage rates into (or out of) the system than prompt neutrons. The effective delayed neutron fraction is calculated as,

$$BETA(h) = \frac{\sum_{iso}\left[\sum_i \beta_{iso}(h)\bar{\chi}_{d,iso}(i,h)\Psi^\dagger(i)\cdot\sum_i \nu\bar{\sigma}_{f,iso}(i)\bar{N}_{iso}\Psi(i)\right]}{\sum_{iso}\left\{\left(1-\sum_h \beta_{iso}(h)\right)\left(\sum_i \bar{\chi}_{p,iso}(i)\Psi^\dagger(i)\right)+\sum_h \beta_{iso}(h)\left(\sum_i \bar{\chi}_{d,iso}(i,h)\Psi^\dagger(i)\right)\right\}\cdot\sum_i \nu\bar{\Sigma}_f(i)\Psi(i)}$$

$$\cong \frac{\sum_{iso}\left[\sum_i \beta_{iso}(h)\bar{\chi}_{d,iso}(i,h)\Psi^\dagger(i)\cdot\sum_i \nu\bar{\sigma}_{f,iso}(i)\bar{N}_{iso}\Psi(i)\right]}{\sum_i \bar{\chi}(i)\Psi^\dagger(i)\cdot\sum_i \nu\bar{\Sigma}_f(i)\Psi(i)}$$

$$\cong \frac{\sum_{iso}\left[\sum_i \beta_{iso}(h)\bar{\chi}_{d,iso}(i,h)\Psi^\dagger(i)\cdot\sum_i \nu\bar{\sigma}_{f,iso}(i)\bar{N}_{iso}\Psi(i)\right]}{k^\dagger\sum_i \nu\bar{\Sigma}_f(i)\Psi(i)}$$

where the summation over *iso* includes the isotopes: Th-232, U-233, U-234, U-235, U-236, U-238, Pu-239, Pu-240, Pu-241, and Pu-242; $\bar{\chi}_{d,iso}(i,h)$ is the delayed neutron fission spectrum from energy group *i* to delayed group *h*, for isotope *iso*; $\bar{\chi}_{p,iso}(i)$ is the prompt neutron fission spectrum for isotope *iso*; and $\bar{\chi}(i)$ is the total fission spectrum for the homogeneous system. The adjoint flux, $\Psi^\dagger(i)$, is obtained by solving the adjoint form of the fundamental mode equation,

$$\bar{\Sigma}_{tr}\Psi^\dagger(i) = \sum_{i'}\left[\bar{\Sigma}_s(i\rightarrow i') + \frac{\nu\bar{\Sigma}_f(i)}{k^\dagger}\cdot\bar{\chi}(i')\right]\Psi^\dagger(i')$$

where B^2 is the value of the material buckling from the solution to the forward form of the fundamental mode calculation; and the adjoint eigenvalue is given by,

$$k^\dagger = \sum_{i'}\bar{\chi}(i')\Psi^\dagger(i')$$

[[

]]

BETA : effective delayed neutron fraction for delayed group h

$$BETAC(h) \cong \frac{\sum_{iso}\left[\sum_{i}\beta_{iso}(h)\bar{\chi}_{d,iso}(i,h)\Psi^{\dagger}(i)\cdot\sum_{i}\nu\bar{\sigma}_{f,iso}(i)\bar{N}_{iso}\Psi(i)\right]}{k^{\dagger}\sum_{i}\nu\bar{\Sigma}_{f}(i)\Psi(i)}$$

with the adjoint flux calculated without the consideration of leakage.

BETAT : effective delayed neutron fraction (summed over 6 delayed groups)

$$BETAT = \sum_{h=1}^{6} BETA(h)$$

BETACT : alternate effective delayed neutron fraction (summed over 6 delayed groups)

$$BETACT = \sum_{h=1}^{6} BETAC(h)$$

C41 : lattice-averaged atomic number density of Pu-241

$$C41 = ADBI(m_{Pu-241} = 26)$$

CDFNN : few-group flux discontinuity factor for narrow-narrow (NN) corner

$$CDFNN(g) = \frac{\psi(g, s = NN)}{\frac{1}{V_{ass}}\int_{V_{ass}} \phi(g,r)dr}$$

where $\psi(g, s = NN)$ is the few-group surface scalar flux in the southeast (Narrow-Narrow) corner of the problem.

CDFNW : few-group flux discontinuity factor for narrow-wide (NW) corner

$$CDFNW(g) = \frac{\psi(g, s = NW)}{\frac{1}{V_{ass}}\int_{V_{ass}} \phi(g,r)dr}$$

where $\psi(g, s = NW)$ is the few-group surface scalar flux in the southwest (Narrow-Wide) corner of the problem. For diagonally symmetric lattices, this will also be the flux in the northeast corner of the problem. (LANCR02 is not limited to diagonally symmetric lattices.)

CDFWN : few-group flux discontinuity factor for wide-narrow (WN) corner

$$CDFWN(g) = \frac{\psi(g, s = WN)}{\frac{1}{V_{ass}} \int_{V_{ass}} \phi(g, r) dr}$$

where $\psi(g, s = WN)$ is the few-group surface scalar flux in the northeast (Wide-Narrow) corner of the problem. For diagonally symmetric lattices, this will also be the flux in the southwest corner of the problem. (LANCR02 is not limited to diagonally symmetric lattices.)

CDFWW : few-group flux discontinuity factor for wide-wide (WW) corner

$$CDFWW(g) = \frac{\psi(g, s = WW)}{\frac{1}{V_{ass}} \int_{V_{ass}} \phi(g, r) dr}$$

where $\psi(g, s = WW)$ is the few-group surface scalar flux in the northwest (Wide-Wide) corner of the problem.

D : few-group lattice-averaged diffusion coefficient

$$D(g) = \sum_{i \in g} \left\{ \frac{\int_{V_{ass}} \phi(g, r) dr}{3 \int_{V_{ass}} \Sigma_{tr}(i, r) \phi(i, r) dr} \right\}$$

where the lattice-averaged diffusion coefficient is calculated in the fine-group energy structure and collapsed directly to the few-group energy structure.

D41 : absorption reaction rate of Pu-241

$$D41 = \sum_{g} \int_{V_{ass}} N_{Pu-241}(r) \sigma_{a,Pu-241}(g) \phi_g(r) dr$$

DK41 : atomic number density reactivity coefficient of Pu-241

$$DK41 = dK / dN_{Pu-241} - dK / dN_{Am-241} = KINF \times \left(\frac{REALL(m_{Pu-241})}{ADBI(m_{Pu-241})} - \frac{REALL(m_{Am-241})}{ADBI(m_{Am-241})} \right)$$

DNFA : lattice-averaged initial heavy metal density (g/cc)

$$DNFA = \sum_{iso} A_{iso} \times ADBI_{iso} / N_{Avogadro}$$

EPF : effective release energy per fission

$$EPF = \frac{\int_{V_{fuel}} \left\{ E_{kinetic}(r) + E_{\gamma}(r) + E_{\beta}(r) - E_{c}(r) \right\} dr}{\sum_{g} \int_{V_{fuel}} \Sigma_{f}(g,r)\phi(g,r)dr}$$

where the energy terms are defined in equations (66) through (69).

EX : exposure point in depletion calculation

EX is the exposure array that corresponds to all other arrays in the binary output file. It is a two dimensional array as a function of time step and void fraction.

FDFN : few-group flux discontinuity factor along narrow gap

$$FDFN(g) = \frac{\frac{1}{S_{narrow}} \int_{S_{narrow}} \psi(g,s)ds}{\frac{1}{V_{ass}} \int_{V_{ass}} \phi(g,r)dr}$$

FDFW : few-group flux discontinuity factor along wide gap

$$FDFW(g) = \frac{\frac{1}{S_{wide}} \int_{S_{wide}} \psi(g,s)ds}{\frac{1}{V_{ass}} \int_{V_{ass}} \phi(g,r)dr}$$

FDR : fission detector response

$$FDR = \sum_{i} \sigma_{f,m_{U-235}}(i)\phi(i, r = SE)$$

where $\phi(i, r = SE)$ is the fine-group scalar flux in the SE corner of the problem; and $\sigma_{f,U-235}(i)$ is the fine-group microscopic fission cross section for U-235.

FFI : lattice-averaged fission fraction of TGBLA isotope m (with GEBLA index)

$$FFI_{m} = \frac{\sum_{g} \int_{V_{ass}} N_{m}(r)\sigma_{f,m}(g,r)\phi(g,r)dr}{\sum_{g} \int_{V_{ass}} \Sigma_{f}(g,r)\phi(g,r)dr}$$

FFILNC : lattice-averaged fission fraction of LANCR isotope m (with LANCR index)

Same definition as FFI.

FFXR : fast flux fraction above 1 MeV

$$FFXR = \frac{\left(\frac{1}{\int_{V_{ass}} dr}\right)\int_{V_{ass}} \phi(E > 1\ \text{MeV})dr}{\left(\frac{1}{\int_{V_{ass}} dr}\right)\int_{V_{ass}} \phi(E > E_2)dr}$$

where E_2 is the upper boundary of the 2nd coarse mesh energy group (see Table A-4).

FLODAT : flow related data (e.g., areas, densities, wetted perimeters, etc.)

FLODAT(1) = in-channel flow area (not including water rods) (cm^2).
FLODAT(2) = out-channel flow area (not including control blade) (cm^2).
FLODAT(3) = water rod flow area (cm^2).
FLODAT(4) = control blade flow area (cm^2).
FLODAT(5) = total flow area (cm^2).
FLODAT(6) = density of in-channel water (g/cm^3).
FLODAT(7) = density of out-channel water (g/cm^3).
FLODAT(8) = density of water in water rods (g/cm^3).
FLODAT(9) = density of water in control blade (g/cm^3).
FLODAT(10) = lattice-averaged water density (g/cm^3).
FLODAT(11) = heated perimeter of all fuel rods (cm).
FLODAT(12) = wetted perimeter of in-channel coolant (cm).
FLODAT(13) = hydraulic diameter of in-channel coolant (cm).

FLUX1 : lattice-averaged fast flux (above 1 MeV)

$$FLUX1 = FFXR \cdot FNF$$

FLUX1C : fast flux (above 1 MeV) in the cladding of rod (x,y)

$$FLUX1C(I,J) = FNF \cdot \frac{\left(\frac{1}{\int_{V_{clad}} dr}\right) \int_{V_{clad}} \phi(E > 1 \text{ MeV}) dr}{\left(\frac{1}{\int_{V_{ass}} dr}\right) \int_{V_{ass}} \phi(E > E_2) dr}$$

where E_2 is the upper boundary of the 2nd coarse mesh energy group (see Table A-4).

FLUXS : lattice-averaged absolute neutron flux

$$FLUXS = \sum_g AVLATF(g)$$

FLXLIB : fine-group critical spectrum from fundamental mode calculation

$$FLXLIB(i) = \Psi(i)$$

where $\Psi(i)$ is the flux from the solution to Eq. (34).

FNF : flux normalization factor

$$FNF = \frac{\sum_i \int_{V_{ass}} \Sigma_f(i,r)\phi(i,r) dr}{\int_{V_{ass}} dr}$$

Factor used to ratio the detector responses.

FRR : relative fission rate in rod (x,y)

$$FRR(x,y) = \frac{\sum_g \int_{V_{x,y}} \Sigma_f(g,r)\phi(g,r) dr}{\left\{\frac{\sum_g \int_{V_{fuel}} \Sigma_f(g,r)\phi(g,r) dr}{\int_{V_{fuel}} dr}\right\}}$$

GMNAME : gamma cross section library name

Name of the gamma cross section library used for this statepoint. Only the first 40 characters of the name are saved.

GRR : relative gamma heating rate for rod (x,y)

$$GRR(x,y) = \frac{\sum_j \int_{V_{x,y}} \Sigma_e(j,r)\phi(j,r)dr}{\left\{ \frac{\sum_j \int_{V_{fuel}} \Sigma_e(j,r)\phi(j,r)dr}{\int_{V_{fuel}} dr} \right\}}$$

where $\Sigma_e(j,r)$ is the macroscopic gamma energy deposition cross section for material region r.

[[

]]

[[

]]

KINF : infinite multiplication factor

This is the multiplication factor obtained from the fine-group fundamental mode calculation following the two-dimensional MoC transport calculation.

KINF3G : few-group infinite multiplication factor

This is the multiplication factor obtained from the few-group cross sections. The few-group cross sections are created using the fine-group critical flux spectrum from the fundamental mode calculation.

$$KINF3G = \frac{\nu\bar{\Sigma}_f(1) + \nu\bar{\Sigma}_f(2)\cdot SI(2) + \nu\bar{\Sigma}_f(3)\cdot SI(3)}{\bar{\Sigma}_a(1) + \bar{\Sigma}_r(1)}$$

where the spectral indices are defined as,

$$SI(2) = \frac{\bar{\Sigma}_r(1)}{\bar{\Sigma}_a(2) + \bar{\Sigma}_r(2)}$$

and

$$SI(3) = \frac{\bar{\Sigma}_r(2)}{\bar{\Sigma}_a(3)}\cdot SI(2)$$

LBNAME : name of neutron cross section library used for this state point

Only the first 40 characters of the name are used.

LNCR_INFO : LANCR02 information

DTIME = Time of execution (beginning of run).

UNAME = User name.

LNCRVR = LANCR02 version.

LBPATH = Library path name (cLibPath).

LBNAME = Name of neutron cross section file (cLibName).

LBLIST = Name of file defining nuclides contained in neutron cross section library (cLibList).

LBVERS = Cross section version (e.g., ENDF/B-VI, ENDF/B-VII, etc.).

GMNAME = Name of gamma cross section library (cGammaLib).

LNCRCM = 5 lines of comments available to the programmer.

MEVPF: Heat deposition factors in internal structures from neutron slowing down (MeV per fission)

The energy deposition due to neutron slowing down in region m, Qm, is given by

$$Q_m = \frac{\sum_{g=1}^{G}\sum_{g'=g+1}^{G}\left(E_g - E_{g'}\right)\int_{V_m} N(r)\sigma_s(g \to g',r)\phi(g,r)dr}{\sum_{g=1}^{G}\int_{V_m} N(r)\sigma_f^g(r)\phi(g,r)dr}$$

where Eg = midpoint energy for energy group g (where Eg' < Eg when g' > g), G=number of energy groups, $N(r)\sigma_s(g \to g',r)$ is the macroscopic scattering cross section from group g to g' at r, $N(r)\sigma_f^g(r)$ is the macroscopic fission cross section in group g at r, Φ(g,r) is the g-group fundamental mode leakage corrected flux at r, and Vm is the volume of region m. The energy deposition calculated with the equation is summed for each region type (cladding, channels, and water rods), providing heat deposition factors for neutron slowing down. The gamma energy deposition is treated separately, as described in Equation (45) of the LTR. Therefore, the gamma energy deposition factors calculation does not include the energy deposition from slowing down of neutrons.

Energy deposition due to neutron slowing down is a function of flux and atomic number densities, which are exposure dependent, and therefore atomic number densities and flux are updated accordingly.

1. Total energy deposited in coolant, gap, fuel, channel and additional coolant on the edge rods:
$$E_{All-Lattice} \equiv \sum_{j \in All-Lattice}\left[Q_j\right]$$
2. Energy deposited in coolant (in-channel water, excluding rods water):
$$E_{COO} \equiv \sum_{j \in COO}\left[Q_j\right]$$
3. Energy deposited in gap (out-channel, wings and rods water):
$$E_{MOD} \equiv \sum_{j \in MOD}\left[Q_j\right]$$
4. Energy deposited in fuel:
$$E_{FUE} \equiv \sum_{j \in FUE}\left[Q_j\right]$$
5. Energy deposited in channel:
$$E_{\{BOX,CAN\}} \equiv \sum_{j \in \{BOX,CAN\}}\left[Q_j\right]$$
6. Energy deposited in additional structure such as coolant on the edge rods.

$$E_{rest} \equiv E_{All-Lattice} - E_{COO} - E_{MOD} - E_{FUE} - E_{\{BOX,CAN\}}$$

LANCR02 does not provide the heat deposited in spacers since they are not explicitly modeled as part of the lattice. Heat deposition in bundle structures due to gamma energy deposition is described in Section 2.6.1.

MOCINP : card input from MoC module

A copy of the ASCII card input for the MoC solution.

POLAT : power density

Input power density (kW/L).

RCRA : neutron flux ratio of narrow-narrow corner rod to lattice average

$$RCRA(g) = \frac{\phi(g, r = SE)}{AVLATF(g)}$$

where $\phi(g, r = SE)$ is the few-group scalar flux in the SE corner of the problem.

REALL : reactivity worth of each nuclide

Reactivity change when the atomic number density of each nuclide increases 100%.

$$REALL(m_{iso}) = \frac{\sum_g \int_{V_{ass}} N_{iso} \nu\sigma_{f,iso}(g,r)\phi(g,r)dr}{\sum_g \int_{V_{ass}} \nu\Sigma_f(g,r)\phi(g,r)dr} - \frac{\sum_g \int_{V_{ass}} N_{iso}\sigma_{a,iso}(g,r)\phi(g,r)dr}{\sum_g \int_{V_{ass}} \Sigma_a(g,r)\phi(g,r)dr}$$

REB10 : reactivity worth of B-10

$$REB10 = REALL(m_{B-10} = 41)$$

REGD : reactivity worth of Gd-155 and Gd-157

$$REGD = REALL(m_{Gd-155} = 149) + REALL(m_{Gd-157} = 151)$$

RESM : reactivity worth of Sm-149

$$RESM = REALL(m_{Sm-149} = 133)$$

REXE : reactivity worth of Xe-135

$$REXE = REALL(m_{Xe-135} = 98)$$

REX : rod-wise relative exposure

$$REX(x,y) = \frac{\text{expo}(x,y)}{\left\{ \frac{\int_{V_{fuel}} \text{expo}(x,y)dr}{\int_{V_{fuel}} dr} \right\}}$$

where $\text{expo}(x,y)$ is the integrated energy produced by the pin (in GWd) divided by the initial weight of actinides in the pin (in short tons).

RHOB : reference water density (g/cc)

$$RHOB = 0.73749$$

This is a reference water density constant used in many GE processes. The value is based on the saturated water density at 286 C, and is used to normalize the water density edits (e.g. U, UH, UIN, UOUT, UWR).

RPR : rod-wise relative power

$$RPR(x,y) = \frac{pow(x,y)}{\left\{ \frac{\int_{V_{fuel}} pow(x,y)dr}{\int_{V_{fuel}} dr} \right\}}$$

RTIPA : ratio of TIP flux to lattice-averaged flux for few-group energy g

$$RTIPA(g) = \frac{\phi(g, r = SE)}{AVLATF(g)}$$

SAAM41 : lattice-averaged microscopic absorption cross section of Am-241

$$SAAM41(g) = \frac{\int_{V_{ass}} N_{Am-241}(r)\sigma_{a,Am-241}(g,r)\phi(g,r)dr}{\frac{1}{V_{ass}} \int_{V_{ass}} N_{Am-241}(r)dr \int_{V_{ass}} \phi(g,r)dr}$$

SAPU41 : lattice-averaged microscopic absorption cross section of Pu-241

$$SAPU41(g) = \frac{\int_{V_{ass}} N_{Pu-241}(r)\sigma_{a,Pu-241}(g,r)\phi(g,r)dr}{\frac{1}{V_{ass}}\int_{V_{ass}} N_{Pu-241}(r)dr \int_{V_{ass}} \phi(g,r)dr}$$

SASM : lattice-averaged microscopic thermal absorption cross section of Sm-149

$$SASM = \frac{\int_{V_{ass}} N_{Sm-149}(r)\sigma_{a,Sm-149}(3,r)\phi(3,r)dr}{\frac{1}{V_{ass}}\int_{V_{ass}} N_{Sm-149}(r)dr \int_{V_{ass}} \phi(3,r)dr}$$

SCPU40 : lattice-averaged microscopic capture cross section of Pu-240

$$SCPU40(g) = \frac{\int_{V_{ass}} N_{Pu-240}(r)\sigma_{c,Pu-240}(g,r)\phi(g,r)dr}{\frac{1}{V_{ass}}\int_{V_{ass}} N_{Pu-240}(r)dr \int_{V_{ass}} \phi(g,r)dr}$$

SAXE : lattice-averaged microscopic thermal absorption cross section of Xe-135

$$SAXE = \frac{\int_{V_{ass}} N_{Xe-135}(r)\sigma_{a,Xe-135}(3,r)\phi(3,r)dr}{\frac{1}{V_{ass}}\int_{V_{ass}} N_{Xe-135}(r)dr \int_{V_{ass}} \phi(3,r)dr}$$

SFPU41 : lattice-averaged microscopic fission cross section of Pu-241

$$SFPU41(g) = \frac{\int_{V_{ass}} N_{Pu-241}(r)\sigma_{f,Pu-241}(g,r)\phi(g,r)dr}{\frac{1}{V_{ass}}\int_{V_{ass}} N_{Pu-241}(r)dr \int_{V_{ass}} \phi(g,r)dr}$$

SPPU41 : lattice-averaged microscopic production cross section of Pu-241

$$SPPU41(g) = \frac{\int_{V_{ass}} N_{Pu-241}(r)\nu\sigma_{f,Pu-241}(g,r)\phi(g,r)dr}{\frac{1}{V_{ass}}\int_{V_{ass}} N_{Pu-241}(r)dr \int_{V_{ass}} \phi(g,r)dr}$$

STATUS : final status of job

CLEAN = normal termination; blank = abnormal termination

TASD : Time after shutdown

LANCR02 input data TASD.

TEF : fuel temperature

LANCR02 input data.

TEMC : cladding temperature

LANCR02 input data.

TEMF : fuel temperature

LANCR02 input data.

TEM : in-channel coolant temperature

LANCR02 input data.

TEMOUT : out-channel coolant temperature

LANCR02 input data TEMPO.

U : instantaneous relative water density

$$U = \frac{\int_{V_{ass}} \rho_{H_2O}(r)dr}{RHOB\ V_{H_2O}}$$

where V_{H_2O} is the volume of all in-channel and out-channel water.

UH : exposure-averaged relative water density

$$UH = \frac{\int_0^E U(E')dE'}{\int_0^E dE'}$$, where E and E' are exposures.

UIN : instantaneous in-channel relative water density

$$UIN = \frac{FLODAT(6)}{RHOB}$$

UOUT : instantaneous out-channel relative water density

$$UOUT = \frac{FLODAT(7)}{RHOB}$$

UWR : instantaneous water rod relative water density

$$UWR = \frac{FLODAT(8)}{RHOB}$$

V : average few-group neutron velocity

$$V(g) = \frac{\sum_{i \in g} \Psi^{\dagger}(i)}{\sum_{i \in g} \frac{\Psi^{\dagger}(i)}{v(i)}}$$

where $v(i)$ is the neutron velocity in the fine-group energy structure; and $\Psi^{\dagger}(i)$ is the adjoint flux from the fundamental mode solution (see the description for BETA(h) in this section).

V,OPT2 : average few-group neutron velocity (calculated using critical forward flux)

$$V(g) = \frac{\sum_{i \in g} \Psi(i)}{\sum_{i \in g} \frac{\Psi(i)}{v(i)}}$$

where $\Psi(i)$ is the critical forward flux from the fundamental mode solution.

V,OPT3 : average few-group neutron velocity (calculated using infinite adjoint flux)

$$V(g) = \frac{\sum_{i \in g} \Psi^{\dagger}(i)}{\sum_{i \in g} \frac{\Psi^{\dagger}(i)}{v(i)}}$$

where $\Psi^{\dagger}(i)$ is the infinite adjoint flux from the fundamental mode solution (no neutron leakage included).

VF : void fraction

LANCR02 input data.

VFIN : Void fraction

LANCR02 input data.

VFOUT : Void fraction

LANCR02 input data.

VFWR : Void fraction

LANCR02 input data.

VFXY : Pin-wise void fraction

This is the pin-wise void distribution used during the MoC solution. For most applications, the void is uniformly distributed across the in-channel area. However, the user has the option of entering a non-uniform void distribution or instructing the code to calculate a non-uniform void distribution based on distributed void model.

WFI : lattice-averaged weight fraction of GTHERM isotope to initial heavy elements (with GEBLA index)

$$WFI(m_{iso}) = \frac{\int_{V_{ass}} A_{iso} N_{iso}(r) dr}{\sum_{iso=1}^{30} \int_{V_{ass}} A_{iso} N_{iso}^{BOL}(r) dr}$$

where the value of *m* for heavy metals encompasses Th-228 through Am-242.

WFILNC : lattice-averaged weight fraction of GTHERM isotope to initial heavy elements (with LANCR index)

$$WFI(m_{iso}) = \frac{\int_{V_{ass}} A_{iso} N_{iso}(r) dr}{\sum_{iso=1}^{40} \int_{V_{ass}} A_{iso} N_{iso}^{BOL}(r) dr}$$

where the value of *m* for heavy metals encompasses Th-228 through Cm-246.

XA : few-group lattice-averaged absorption cross section

$$XA(g) = \frac{\sum_{i \in g} \int_{V_{ass}} \Sigma_a(i,r)\phi(i,r)dr}{\sum_{i \in g} \int_{V_{ass}} \phi(i,r)dr}$$

XAMXE : lattice-averaged thermal absorption cross section minus the Xe contribution

$$XAMXE = XA(g) - SAXE \times ADBI_{m=98}$$

XF : few-group lattice-averaged fission cross section

$$XF(g) = \frac{\sum_{i \in g} \int_{V_{ass}} \Sigma_f(i,r)\phi(i,r)dr}{\sum_{i \in g} \int_{V_{ass}} \phi(i,r)dr}$$

XFCRT : microscopic fission cross section at instrument location

$$XFCRT(g) = \frac{\sum_{i \in g} \sigma_{f,U-235}(i)\phi(i,r')}{\sum_{i \in g} \phi(i,r')}$$

where r' is the location of the instrument tube in the SE water gap corner of the problem. The microscopic fission cross section is the unshielded (i.e., infinitely dilute) value.

XNF : few-group lattice-averaged production cross section

$$XNF(g) = \frac{\sum_{i \in g} \int_{V_{ass}} \nu\Sigma_f(i,r)\phi(i,r)dr}{\sum_{i \in g} \int_{V_{ass}} \phi(i,r)dr}$$

XSC : few-group lattice-averaged scattering kernel

$$XSC(g',g) = \frac{\sum_{i \in g} \sum_{i' \in g'} \int_{V_{ass}} \Sigma_s(i',i,r)\phi(i',r)dr}{\sum_{i \in g} \sum_{i' \in g'} \int_{V_{ass}} \phi(i',r)dr}$$

where $XSC(g',g)$ is the scattering cross section from group g' to group g.

XSL : few-group lattice-averaged removal cross section

$$XSL(1) = \frac{\nu\bar{\Sigma}_f(1) + \nu\bar{\Sigma}_f(2)\cdot\frac{\bar{\phi}(2)}{\bar{\phi}(1)} + \nu\bar{\Sigma}_f(3)\cdot\frac{\bar{\phi}(3)}{\bar{\phi}(1)}}{k^{\infty}} - \bar{\Sigma}_a(1)$$

$$XSL(2) = XSL(1)\cdot\frac{\bar{\phi}(1)}{\bar{\phi}(2)} - \bar{\Sigma}_a(2)$$

$$XSL(3) = 0$$

where the few-group eigenvalue is calculated as,

$$k^{\infty} = \frac{\nu\bar{\Sigma}_f(1)\cdot\bar{\phi}(1) + \nu\bar{\Sigma}_f(2)\cdot\bar{\phi}(2) + \nu\bar{\Sigma}_f(3)\cdot\bar{\phi}(3)}{\bar{\Sigma}_a(1)\cdot\bar{\phi}(1) + \bar{\Sigma}_a(2)\cdot\bar{\phi}(2) + \bar{\Sigma}_a(3)\cdot\bar{\phi}(3)}$$

[[

]]

XTRLIB : fine-group lattice-averaged transport cross section

$$XTRLIB(i) = \frac{\int_{V_{ass}} \Sigma_{tr}(i,r)\phi(i,r)dr}{\int_{V_{ass}} \phi(i,r)dr}$$

XYLOC : location of fuel pin relative to wide-wide corner

XYLOC(1,x,y) : x-coordinate of pin (x,y)

XYLOC(2,x,y) : y-coordinate of pin (x,y)

YBA140 : average fission yield of Ba-140

$$YBA140 = \frac{\sum_{iso=1}^{40}\int_{V_{fuel}} Y_{iso,Ba-140}N_{iso}(r)\sigma_{f,iso}(g,r)\phi(g,r)dr}{\sum_{iso=1}^{40}\int_{V_{fuel}} N_{iso}(r)\sigma_{f,iso}(g,r)\phi(g,r)dr}$$

where $Y_{iso,Ba-140}$ is the yield from actinide *iso* to Ba-140; and the summation is performed over all actinides Th-228 through Cm-246.

YCE140 : average fission yield of Ce-144

$$YCE140 = \frac{\sum_{iso=1}^{40} \int_{V_{fuel}} Y_{iso,Ce-144} N_{iso}(r) \sigma_{f,m'} iso(g,r) \phi(g,r) dr}{\sum_{iso=1}^{40} \int_{V_{fuel}} N_{iso}(r) \sigma_{f,iso}(g,r) \phi(g,r) dr}$$

where $Y_{iso,Ce-144}$ is the yield from actinide iso to Ce-144; and the summation is performed over all actinides Th-228 through Cm-246.

YI : average fission yield of I-135

$$YI = \frac{\sum_{iso=1}^{40} \int_{V_{fuel}} Y_{iso,I-135} N_{iso}(r) \sigma_{f,iso}(g,r) \phi(g,r) dr}{\sum_{iso=1}^{40} \int_{V_{fuel}} N_{iso}(r) \sigma_{f,iso}(g,r) \phi(g,r) dr}$$

where $Y_{iso,I-135}$ is the yield from actinide iso to I-135; and the summation is performed over all actinides Th-228 through Cm-246.

YPM : average fission yield of Pm-149

$$YPM = \frac{\sum_{iso=1}^{40} \int_{V_{fuel}} Y_{iso,Pm-149} N_{m'}(r) \sigma_{f,iso}(g,r) \phi(g,r) dr}{\sum_{iso=1}^{40} \int_{V_{fuel}} N_{iso}(r) \sigma_{f,iso}(g,r) \phi(g,r) dr}$$

where $Y_{iso,Pm-149}$ is the yield from actinide iso to Pm-149; and the summation is performed over all actinides Th-228 through Cm-246.

YRU105 : average fission yield of Ru-105

$$YRU105 = \frac{\sum_{iso=1}^{40} \int_{V_{fuel}} Y_{iso,Ru-105} N_{iso}(r) \sigma_{f,iso}(g,r) \phi(g,r) dr}{\sum_{iso=1}^{40} \int_{V_{fuel}} N_{iso}(r) \sigma_{f,iso}(g,r) \phi(g,r) dr}$$

where $Y_{iso,Ru-105}$ is the yield from actinide iso to Ru-105; and the summation is performed over all actinides Th-228 through Cm-246.

YXE : average fission yield of Xe-135

$$YXE = \frac{\sum_{iso=1}^{40} \int_{V_{fuel}} Y_{iso,Xe-135} N_{iso}(r) \sigma_{f,iso}(g,r) \phi(g,r) dr}{\sum_{iso=1}^{40} \int_{V_{fuel}} N_{iso}(r) \sigma_{f,iso}(g,r) \phi(g,r) dr}$$

where $Y_{iso,Xe-135}$ is the yield from actinide *iso* to Xe-135; and the summation is performed over all actinides Th-228 through Cm-246.

9. MODEL UPDATES

GNF is committed to providing state-of-the-art reactor analysis codes. This commitment is in agreement with NUREG-0800, which requires that analytical methods and database should be representative of the state-of-the-art. LANCR02 is a controlled computer code under the ECP quality assurance requirements.

All code changes will be reported to the Licensee(s) for their use in preparing 10CFR50.59 evaluations. However, to effectively manage the future viability of LANCR02 as inputs to downstream analyses, GNF proposes the following requirements for modifications in the use of or to the approved LANCR02 code. All changes to a particular version will be documented within the ECP change and qualification documentation described in Section 9.3.

9.1. Updates to the Basic Nuclear Data

Updates to the basic nuclear data will not be considered to constitute a departure from a method of evaluation and such changes may be made without NRC review and approval as long as the performance relative to the current qualification basis is not adversely affected.

- [[

]]

9.2. Updates to the Model Implementation

While the methodology as outlined in this document is not to be changed, modifications to the implementation of the methodology as encoded in LANCR02 may be made as needed to facilitate processing of new requirements.

[[

]]

Updates to the model implementation will not be considered to constitute a departure from a method of evaluation and such changes may be made without NRC review and approval, as long as the performance relative to the current qualification basis is not adversely affected. [[

]]

9.3. Testing Requirements

[[

]]

10. APPLICABLE DOCUMENTATION

[1] D. Knott, et al., "Description of the LANCER02 Lattice Physics Code for Single-Assembly and Multibundle Analysis," *Nucl. Sci. Eng.*, Vol. 155, p. 331-354, (2007).

[2] R. E. MacFarlane, "NJOY99.0, Code System for Producing Pointwise and Multigroup Neutron and Photon Cross Sections from ENDF/B Data," PSR-480, Los Alamos National Laboratory, Los Alamos, N.M. (2000).

[3] R. J. J. Stammler and M. J. Abbate, *Methods of Steady-State Reactor Physics in Nuclear Design*, Academic Press (1983).

[4] E.P. Wigner, et al., *J. Appl. Phys*., Vol. 2, pp. 257, 260, 271, (1955).

[5] C. C. Stoker and Z. J. Weiss, "Spatially Dependent Resonance Cross Sections in a Fuel Rod," *Ann. Nucl. Energy*, Vol. 23, No. 9, pp. 765-778 (1996).

[6] N. Sugimura and A. Yamamoto, "Evaluation of Dancoff Factors in Complicated Geometry Using the Method of Characteristics," *J. Nucl. Sci. Tech.*, Vol. 43, No. 10, pp. 1182-1187 (2006).

[7] A. Hébert, "A Review of Legacy and Advanced Self-Shielding Models for Lattice Calculations," *Intl. Topl. Mtg. on Math. & Comp*., Avignon, France, (2005).

[8] M. L. Williams, "Correction of Multigroup Cross Sections for Resolved Resonance Interference in Mixed Absorbers," *Nucl. Sci. Eng.*, Vol. 83, p. 37-40 (1983).

[9] E. Wehlage, et al., "Modeling Resonance Interference Effects in the Lattice Physics Code LANCER02," *Intl. Topl. Mtg. on Math. & Comp*., Avignon, France, (2005).

[10] D. Knott, "KRAM, A Lattice Physics Code for Modeling the Detailed Depletion of Gadolinia Isotopes from BWR Fuel Designs," PhD Thesis, The Pennsylvania State University, University Park, PA, (1991).

[11] I. Carlvik, "Integral Transport Theory in One-Dimensional Geometries," Part of Carlvik's PhD Thesis, Chalmers University, Göteborg, Sweden, AE-227, (1966).

[12] I. Carlvik, "A Method for Calculating Collision Probabilities in General Cylindrical Geometry and Applications to Flux Distributions and Dancoff Factors," Part of Carlvik's PhD Thesis, Chalmers University, Göteborg, Sweden, (1966).

[13] E. E. Lewis and W. F. Miller, Jr., *Computational Methods of Neutron Transport*, John Wiley & Sons, Inc., (1984).

[14] J. R. Askew, "A Characteristics Formulation of the Neutron Transport Equation in Complicated Geometries," AEEW-M 1108, (1972).

[15] A. Yamamoto, M. Tabuchi, N. Sugimura, T. Ushio, and M. Mori, "Derivation of Optimum Polar Angle Quadrature Set for the Method of Characteristics Based on Approximation Error for the Bickley Function," *Journal of Nuclear Science and Technology*, Vol. 44, No. 2, p. 129-136 (2007).

[16] D. Knott and M. Edenius, "Validation of the CASMO-4 Transport Solution," *Proc. of the Joint Intl. Conf. on Math. Meth. and Supercomp. in Nucl. Apps*., Karlsruhe, Germany (1993).

[17] S. Richards (NRC) to G. Watford (GE), MFN-035-99, Amendment 26 to GE Licensing Topical Report NEDE-24011-P-A*,* "*GESTAR II" – Implementing Improved GE Steady State Methods (TAC No. MA6481)*, November 10, 1999.

Appendix A. Neutron Cross Section Library

The library data have been processed by NJOY99.161 using the ENDF/B-VII release 0 evaluation. Energy group dependent neutron cross sections for LANCR02 are contained in a 118-group library. Any isotopes needed by LANCR02 but not contained in the ENDF/B-VII release 0 have been obtained from their most recent ENDF/B-6 release 8 evaluation (this only includes "natural" isotopes). ENDF/B-VII release 0 data is targeted for qualification and production purposes.

The energy group-dependent cross sections span the energy range from 10^{-5} eV to 20 MeV and include data for 38 individual actinides and 99 individual fission products, along with data for an assortment of other elements such as hydrogen, oxygen, boron, carbon, hafnium, zirconium, various elements that comprise stainless steel, etc. Table A-1 to Table A-3 list all isotopes contained in the library. Isotope numbers 1 to 40 are reserved for actinides.

The energy group boundaries for the fine-group library and coarse-group library structure are listed in Table A-4.

Table A-1 Actinides Contained in the Cross Section Library

m	Nuclide	MATID	m	Nuclide	MATID	m	Nuclide	MATID
1	Th228	90228	14	U 238	92238	27	Pu242	94242
2	Th230	90230	15	Np236m	193236	28	Pu243	94243
3	Th231	90231	16	Np236	93236	29	Am241	95341
4	Th232	90232	17	Np237	93237	30	Am242m	195242
5	Pa231	91231	18	Np238	93238	31	Am242	95242
6	Pa232	91232	19	Np239	93239	32	Am243	95243
7	Pa233	91233	20	Np240	93240	33	Am244	95244
8	U 232	92232	21	Pu236	94236	34	Cm242	96242
9	U 233	92233	22	Pu237	94237	35	Cm243	96243
10	U 234	92234	23	Pu238	94238	36	Cm244	96244
11	U 235	92235	24	Pu239	94239	37	Cm245	96245
12	U 236	92236	25	Pu240	94240	38	Cm246	96246
13	U 237	92237	26	Pu241	94241			

Table A-2 Fission Products and Absorbers in the Cross Section Library

m	Nuclide	MATID	m	Nuclide	MATID	m	Nuclide	MATID
41	B 10	5010	90	I 133	53133	139	Sm156	62156
42	B 11	5011	91	I 135	53135	140	Eu152	63152
43	Kr 83	36083	92	Xe131m	154131	141	Eu153	63153
44	Y 93	39093	93	Xe131	54131	142	Eu154	63154
45	Zr 91	40091	94	Xe132	54132	143	Eu155	63155
46	Zr 92	40992	95	Xe133m	154133	144	Eu156	63156
47	Zr 93	40093	96	Xe133	54133	145	Eu157	63157
48	Zr 95	40095	97	Xe134	54134	146	Gd152	64152
49	Zr 96	40096	98	Xe135	54135	147	Gd153	64153
50	Zr 97	40097	99	Cs133	55133	148	Gd154	64154
51	Nb 95m	141095	100	Cs134m	155134	149	Gd155	64155
52	Nb 95	41095	101	Cs134	55134	150	Gd156	64156
53	Mo 95	42095	102	Cs135	55135	151	Gd157	64157
54	Mo 96	42096	103	Cs137	55137	152	Gd158	64158
55	Mo 97	42097	104	Ba134	56134	153	Gd160	64160
56	Mo 98	42098	105	Ba140	56140	154	Tb159	65159
57	Mo 99	42099	106	La139	57139	155	Tb160	65160
58	Mo100	42100	107	La140	57140	156	Tb161	65161
59	Tc 99m	143099	108	La141	157140	157	Dy160	66160
60	Tc 99	43099	109	Ce141	58141	158	Dy161	66161
61	Ru100	44100	110	Ce142	58142	159	Dy162	66162
62	Ru101	44101	111	Ce143	58143	160	Dy163	66163
63	Ru102	44102	112	Ce144	58144	161	Dy164	66164
64	Ru103	44103	113	Pr141	59141	162	Ho165	67165
65	Ru104	44104	114	Pr143	59143	163	Er162	68162
66	Ru105	44105	115	Pr145	159143	164	Er164	68164
67	Ru106	44106	116	Nd142	60142	165	Er166	68166
68	Rh103	45103	117	Nd143	60143	166	Er167	68167
69	Rh105	45105	118	Nd144	60144	167	Er168	68168
70	Pd104	46104	119	Nd145	60145	168	Er170	68170
71	Pd105	46105	120	Nd146	60146	169	Hf174	72174
72	Pd106	46106	121	Nd147	60147	170	Hf175	72175
73	Pd107	46107	122	Nd148	60148	171	Hf176	72176
74	Pd108	46108	123	Nd149	60149	172	Hf177	72177
75	Pd109	46109	124	Nd150	60150	173	Hf178	72178
76	Ag109	47109	125	Pm147	61147	174	Hf179m	172178
77	Ag113	47113	126	Pm148m	161148	175	Hf179	72179
78	Cd110	48110	127	Pm148	61148	176	Hf180	72180
79	Cd111	48111	128	Pm149	61149	177	(Empty)	
80	Cd112	48112	129	Pm150	61150	178	(Empty)	
81	Cd113m	148113	130	Pm151	61151	179	(Empty)	
82	Cd113	48113	131	Sm147	62147	180	PFP1	99991
83	Sb129	51129	132	Sm148	62148	181	PFP2	99992
84	Te129m	152129	133	Sm149	62149	182	(Empty)	
85	Te130	52130	134	Sm150	62150	183	(Internal)	
86	Te131m	152130	135	Sm151	62151	184	(Internal)	
87	I 127	53127	136	Sm152	62152	185	(Internal)	
88	I 129	53129	137	Sm153	62153			
89	I 131	53131	138	Sm154	62154			

Table A-3 Other Isotopes and Natural Elements in the Cross Section Library

m	Nuclide	MATID	m	Nuclide	MATID	m	Nuclide	MATID
186	H 1	1001	200	Cr 53	24053	214	Zr	40000
187	H 2	1002	201	Cr 54	24054	215	Ag107	47107
188	H2O	18	202	Mn 55	25055	216	Cd	48000
189	D2O	20	203	Fe 54	26054	217	In	49000
190	C 12	6012	204	Fe 56	26056	218	Au197	79197
191	N 14	7014	205	Fe 57	26057	219	Li 6	3006
192	N 15	7015	206	Fe 58	26058	220	Li 7	3007
193	O 16	8016	207	Ni 58	28058	221	Be 9	4009
194	Na 23	11023	208	Ni 60	28060	222	Ca	20000
195	Al 27	13027	209	Ni 61	28061	223	K	19000
196	Si	14000	210	Ni 62	28062	224	Cr_nat	24000
197	Ti	22000	211	Ni 64	28064	225	Fe_nat	26000
198	Cr 50	24050	212	Cu 63	29063	226	Ni_nat	28000
199	Cr 52	24052	213	Cu 65	29065			

Elements in red are natural element mixtures taken from the ENDF/B VI.8 library. The ENDF/B VII .0 data only includes isotopic data, not natural elements.

Table A-4 Energy Boundaries of the Fine-Group and Coarse-Group Structures

		Upper Boundary (eV)			Upper Boundary (eV)			Upper Boundary (eV)			Upper Boundary (eV)
1	1	2.0000E+07	31		1.4872E+02	61		1.0710E+00	91		8.6200E-02
2		1.2840E+07	32		1.1864E+02	62	16	1.0450E+00	92		8.0000E-02
3		1.0000E+07	33		9.4642E+01	63		1.0200E+00	93		7.4000E-02
4		7.7880E+06	34		7.5497E+01	64	17	9.5000E-01	94		6.8000E-02
5		6.0653E+06	35		6.4937E+01	65		7.8000E-01	95		6.3000E-02
6		4.7237E+06	36		4.8043E+01	66		6.2500E-01	96	21	5.8000E-02
7		3.6788E+06	37	6	3.7612E+01	67		5.0000E-01	97		5.4000E-02
8		2.8650E+06	38	7	3.5379E+01	68		4.2500E-01	98		5.0000E-02
9		2.2313E+06	39	8	2.7697E+01	69		3.8000E-01	99		4.7000E-02
10		1.7377E+06	40		2.3052E+01	70	18	3.5000E-01	100		4.3500E-02
11		1.3533E+06	41	9	2.1684E+01	71		3.2000E-01	101		4.0000E-02
12	2	8.2085E+05	42	10	2.0397E+01	72		3.0000E-01	102		3.7500E-02
13		4.9787E+05	43	11	1.5968E+01	73		2.8000E-01	103		3.5000E-02
14		3.0197E+05	44		1.2558E+01	74		2.6500E-01	104		3.2500E-02
15		1.8316E+05	45		9.8768E+00	75		2.5000E-01	105		3.0000E-02
16	3	1.1109E+05	46		8.7000E+00	76		2.3500E-01	106		2.7400E-02
17		6.7379E+04	47	12	7.1500E+00	77		2.2000E-01	107	22	2.5000E-02
18		4.8068E+04	48	13	6.7000E+00	78	19	2.0600E-01	108		2.2400E-02
19		2.4788E+04	49	14	6.3000E+00	79		1.9200E-01	109		2.0000E-02
20		1.5034E+04	50		4.0000E+00	80		1.8000E-01	110		1.7400E-02
21		9.1188E+03	51		3.3000E+00	81		1.6900E-01	111		1.5000E-02
22	4	5.5308E+03	52		2.6000E+00	82		1.5900E-01	112		1.2500E-02
23		3.1435E+03	53		2.3500E+00	83		1.5000E-01	113	23	1.0000E-02
24		1.7866E+03	54		2.1000E+00	84		1.4000E-01	114		8.0000E-03
25		1.0155E+03	55		1.8400E+00	85		1.3100E-01	115		6.5000E-03
26		5.7714E+02	56		1.7000E+00	86		1.2200E-01	116		5.0000E-03
27		3.2802E+02	57		1.5000E+00	87		1.1400E-01	117		3.6000E-03
28		2.9298E+02	58		1.3000E+00	88	20	1.0700E-01	118		2.0000E-03
29		2.6167E+02	59		1.1500E+00	89		1.0000E-01			1.0000E-05[1]
30	5	1.8644E+02	60	15	1.0970E+00	90		9.2800E-02			

[[

]]

The three-group boundaries are at 9.1188 keV and 0.625 eV.

[1] Lower boundary of the neutron Library

Appendix B. Gamma Cross Section Library

The gamma cross section library uses 8 energy groups. The energy boundaries of the 8-group gamma energy structure are shown in Table B-1.

Table B-1 Energy Boundaries of the 8-Group Gamma Library

	Upper Boundary (eV)		Upper Boundary (eV)		Upper Boundary (eV)		Upper Boundary (eV)
1	8.5000E+06	3	4.0000E+06	5	2.2000E+06	7	7.5000E+05
2	6.0000E+06	4	3.0000E+06	6	1.4000E+06	8	3.0000E+05
							1.175E+05[2]

The energy boundaries of the final 8-group energy structure are shown in Table B-1. Since the 8-group energy structure is too coarse to be generated directly from continuous energy cross section data, the library was generated using a two-step process.

First, an 80-group energy structure was defined spanning Table B-1, in which each of the 8 energy groups listed in Table B-1 were further sub-divided into 10 groups of equal energy widths. Gamma cross sections were evaluated for each element at each midpoint energy of the 80-groups.

A processing code was used to create 80-group gamma cross sections. In this code, continuous energy gamma cross sections are expressed by formulae based on combined experimental and theoretical data. The sources of the gamma cross sections are the various expressions given in NEDE-23695. Section III.2 and the supporting Table 3.1 from NEDE-23695 are included herein. Since energy variations of gamma cross sections are relatively smooth, a cross section value at the midpoint energies of each 80-group may be taken as the simple average over a group. The resulting gamma cross sections were assumed to be independent over conditions of interest.

The gamma spectrum is affected mainly by heavy elements and is insensitive to the void fraction. Therefore, the gamma spectrum in a BWR remains nearly the same over the commercial BWR fuel bundles from the old to new designs. This fact validates the use of typical gamma spectrum to condense 80-group cross sections into fewer 8 energy groups.

Based on the 80-group cross sections, a single fuel pin cell transport calculation was performed using ANISN (1-D cylinder, isotropic scattering, S8) [Ref. 1]. The resulting gamma spectrum was used as a weighting function to condense cross sections into the target 8-group energy structure. The final 8-group cross section data has been loaded into a file.

During this processing, an energy deposition cross section was defined as,

[2] Lower boundary of the gamma library

$$\sigma_e^{\gamma} = \frac{\sum_{\Gamma \in \gamma} \phi_{\Gamma} \left\{ E_{\Gamma} \sigma_{PE+PC}^{\Gamma} + \sum_{\Gamma' \geq \Gamma} \left(E_{\Gamma} - E_{\Gamma'} \right) \sigma_{CS}^{\Gamma \to \Gamma'} \right\}}{\sum_{\Gamma \in \gamma} \phi_{\Gamma}}$$

where, γ and Γ represent the 8-group and 80-group energy structures, respectively; ϕ_{Γ} is the 80-group gamma flux; E_{Γ} is a midpoint energy of group Γ; σ_{PE+PC}^{Γ} is the sum of the photoelectric and pair creation cross section in the 80-group energy structure; and $\sigma_{CS}^{\Gamma \to \Gamma'}$ is the Compton scattering cross section in the 80-group energy structure.

[1] W. W. Engle, Jr., "ANISN, A One-Dimensional Discrete Ordinates Transport Code with Anisotropic Scattering," ORGDP Report K-1693, Oak Ridge, TN (1967).

[[

]]

[[

]]

[[

]]

[[

]]

[[

]]

[[

]]

[[

]]

[[

]]

[[

]]